Swiss J Geosci (2021) 114:16
https://doi.org/10.1186/s00015-021-00393-7

SGG SGS sc | nat
Swiss Journal of Geosciences

ORIGINAL PAPER Open Access

Eclogitic metamorphism in the Alpine far-west: petrological constraints on the Banchetta-Rognosa tectonic unit (Val Troncea, Western Alps)

Alberto Corno[1*], Chiara Groppo[1], Pietro Mosca[2], Alessandro Borghi[1] and Marco Gattiglio[1]

Abstract

The Banchetta-Rognosa tectonic unit (BRU), covering an area of 10 km^2 in the upper Chisone valley, consists of two successions referred to a continental margin (Monte Banchetta succession) and a proximal oceanic domain (Punta Rognosa succession) respectively. In both successions, Mesozoic meta-sedimentary covers discordantly lie on their basement. This paper presents new data on the lithostratigraphy and the metamorphic evolution of the continental basement of the Monte Banchetta succession. It comprises two meta-sedimentary sequences with minor meta-intrusive bodies preserving their original lithostratigraphic configuration, despite the intense Alpine deformation and metamorphic re-equilibration. Phase equilibrium modeling points to a metamorphic eclogitic peak (D1 event) of 20–23 kbar and 440–500 °C, consistent among three different samples, analyzed from suitable lithologies. The exhumation P–T path is characterized by a first decompression of at least 10 kbar, leading to the development of the main regional foliation (i.e. tectono-metamorphic event D2). The subsequent exhumation stage (D3 event) is marked by a further decompression of almost 7–8 kbar associated with a significant temperature decrease (cooling down to 350–400 °C), implying a geothermal gradient compatible with a continental collision regime. These data infer for this unit higher peak P–T conditions than previously estimated with conventional thermobarometry. The comparison of our results with the peak P–T conditions registered by other neighboring tectonic units allows to interpret the BRU as one of the westernmost eclogite-facies unit in the Alps.

Keywords: Western Alps, Banchetta-Rognosa Unit, Lithostratigraphy, Tectono-metamorphic evolution, P–T isochemical phase diagrams

1 Introduction

In collisional zones, segments of continental and oceanic crusts are subducted to great depths and then exhumed as high to ultra-high pressure (HP/UHP) units (Guillot et al., 2009). This is notably well-recognized for example in the Alps (e.g. Chopin et al., 1991; Compagnoni, 2003; Groppo et al., 2019), Himalayas (e.g. Groppo et al., 2007, 2016; Lanari et al., 2013; Laskowski et al., 2016; O'Brien, 2019), China (e.g. Bolin et al., 1995; Nakamura & Hirajima, 2000; Okay et al., 1989; Zhang et al., 1995) and Norway (e.g. Cuthbert et al., 2000; Hacker et al., 2010; Labrousse et al., 2004; Wain, 1997). Defining the extension, zoning and P–T evolution of such subducted crustal units is of primary importance for interpreting the large-scale processes of continental subduction and exhumation in the orogenic systems (e.g. Burov et al., 2014 and references therein).

Editorial handling: Edwin Gnos.

*Correspondence: alberto.corno@unito.it
[1] Dipartimento Di Scienze Della Terra, Università Degli Studi Di Torino, Torino, Italia
Full list of author information is available at the end of the article

The Western Alps, consisting of a stack of European and Adriatic continental units and Liguria-Piemonte oceanic units (Fig. 1a), show metamorphic peak conditions decreasing from east to west. Alpine peak P–T conditions range from eclogite-facies conditions in the inner part of the belt (Internal Crystalline Massifs, Sesia zone, Zermatt-Saas-like units), with locally coesite-eclogite-facies conditions (Lago di Cignana unit, Internal Piedmont Zone on the left side of the Aosta valley, and Brossasco-Isasca unit, southern Dora Maira massif) to lower greenschist-facies conditions in the more external part (Briançonnais—Houillere zone). Based on the

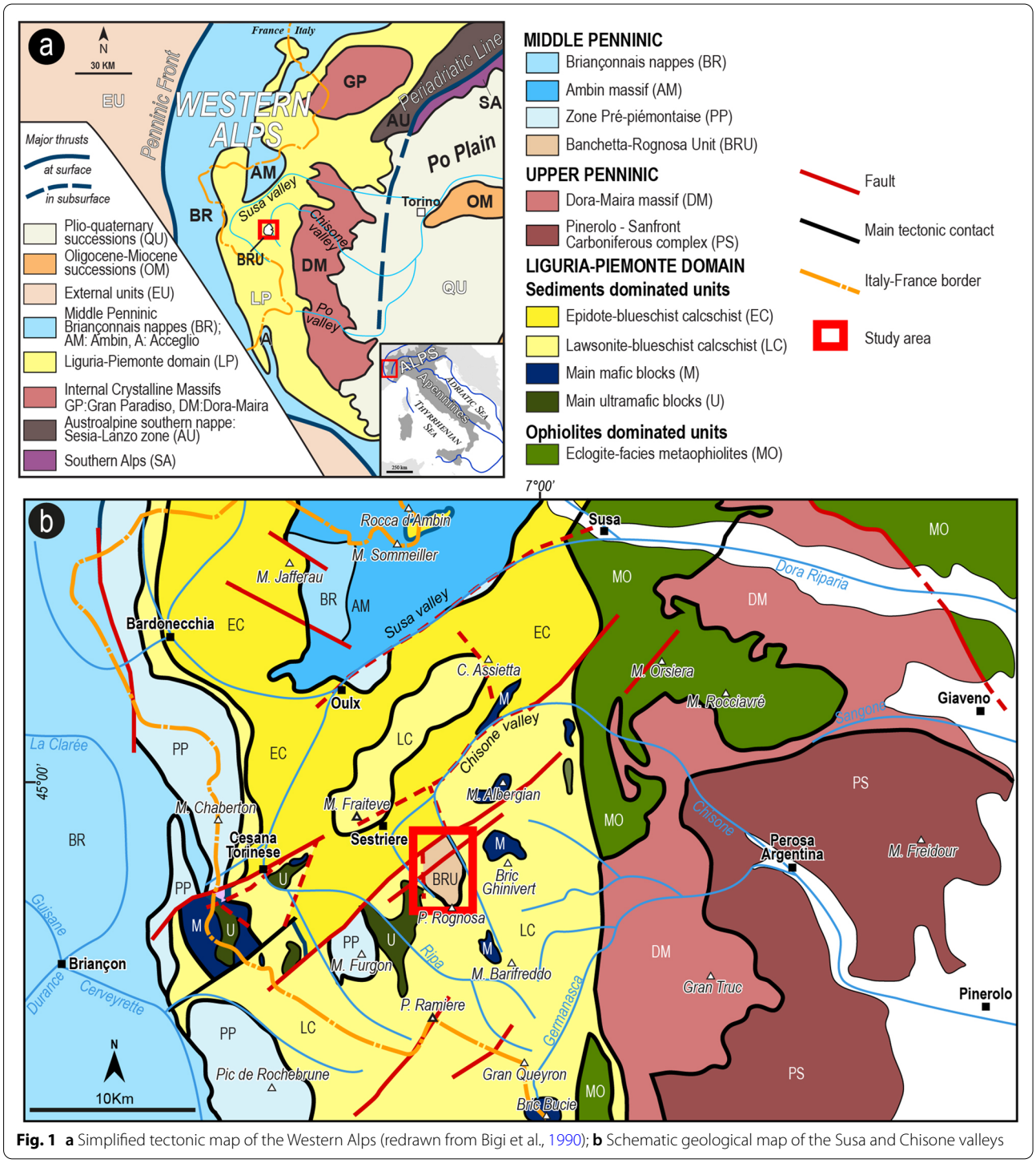

Fig. 1 **a** Simplified tectonic map of the Western Alps (redrawn from Bigi et al., 1990); **b** Schematic geological map of the Susa and Chisone valleys

current state of knowledge, the continental Acceglio-Col Longet nappe (Michard et al., 2003; Schwartz et al., 2000) and the Ambin-Vanoise massifs (Strzerzynski et al., 2012) are the westernmost units (Fig. 1a) presently exhumed within the Liguria-Piemonte domain registering a metamorphic peak at the blueschist to eclogite-facies transition.

This study focuses on the Banchetta-Rognosa tectonic unit (BRU; Corno et al., 2019, 2021), which is a composite unit including continental and oceanic derived rocks, exposed between Chisonetto and Troncea valleys (tributary valleys of the upper Chisone valley, Italian Western Alps; Figs. 1 and 2). According to the available, large-scale, metamorphic maps of the Western Alps (e.g. Ballèvre et al., 2020; Beltrando et al., 2010; Bousquet et al., 2008), the BRU is located in the external part of the belt, characterized by low temperature, high pressure (LT/HP) metamorphism with peak conditions at the blueschist-eclogite-facies transition. However, at present, quantitative studies aimed at estimating the metamorphic peak conditions of the BRU are lacking. This contribution aims at filling this gap: the metamorphic peak conditions registered by the BRU continental basement are quantified using a petrologic approach based on phase equilibria modeling, and the metamorphic evolution of this poorly investigated sector of the Western Alps is constrained for the first time. Finally, the peak P–T conditions recorded in the BRU are compared with peak P–T estimates published for other HP oceanic- and continental-derived units exposed in the proximity of the BRU.

2 Geological overview

The Alpine belt is the result of progressive Late Cretaceous to Eocene subduction of the Alpine Tethys and its adjacent European continental distal margin beneath the Adria plate, leading to continental collision during Late Eocene-Early Oligocene (Coward & Dietrich, 1989; Michard et al., 1996; Stampfli & Marchant, 1997; Lemoine et al., 2000; Dal Piaz, 2010). During the collisional event, deeply subducted continental and oceanic lithospheric segments were exhumed and stacked in the growing mountain belt (Agard et al., 2009; Beltrando et al., 2010; Manzotti et al., 2018; Rubatto & Hermann, 2001).

The metamorphic belt of the Alps (or Axial belt, i.e. between the Penninic Front and the Insubric Line; Polino et al., 1990; Schmid & Kissling, 2000) comprises units classically ascribed to the Penninic and the Austroalpine domains (Fig. 1a). The Austroalpine domain units (i.e. the Sesia–Lanzo zone and the Dent Blanche nappe, e.g. Manzotti et al., 2014a, b) derive from the Adriatic margin; among them, the Eclogitic Micaschist Complex of the Sesia–Lanzo zon is a continental crust basement unit recording syn-orogenic eclogite-facies conditions (e.g. Dal Compagnoni, 1977; Piaz et al., 1972; Regis et al., 2014).

The Penninic domain includes units ascribed to the continental European margin and to the Liguria-Piemonte oceanic basin (Alpine Tethys). The Penninic continental units, in this sector of the Western Alps, consist of: (i) the Internal Crystalline Massifs, which suffered eclogite-facies conditions during subduction (with coesite-eclogite-facies in the Brossasco-Isasca unit of the Southern Dora Maira) (e.g. Chopin et al., 1991; Compagnoni et al., 2012; Gasco et al., 2011; Groppo, et al., 2019; Manzotti et al., 2014a, 2014b) and (ii) the Briançonnais Zone, which identifies a block of continental crust developed during the Jurassic rifting between the two continental plates (Beltrando et al., 2014; Mohn et al., 2010). Within the Briançonnais Zone, the external Briançonnais domain comprises a Carboniferous basement (Houillère zone) metamorphosed at greenschist-facies conditions (Lanari et al., 2012). In the internal Briançonnais domain, the Ambin massif includes two pre-Carboniferous continental basement units, namely the Clarea unit and the overlying Ambin unit, both with Alpine blueschist-facies mineral assemblages (Ganne et al., 2005; Malusà et al., 2002; Polino et al., 2002; Strzerzynski et al., 2012). The Acceglio-Col Longet nappe (Ultrabriançonnais zone), exposed in the southern part of the Western Alps, represents the westernmost HP continental unit, recording a metamorphic peak at the transition between high-T blueschist-facies and low-T eclogite-facies conditions (Michard et al., 2003; Schwartz et al., 2000).

The Liguria-Piemonte domain comprises ophiolite-bearing units with Upper Jurassic to Cretaceous metasedimentary covers (Bearth, 1967; Beltrando et al., 2010 and Balestro et al., 2019 and references therein for a detailed review). At a regional scale, a distinction can be made between eclogitic units (Zermatt-Saas type or Internal Piedmont Zone) and overlying blueschist units (Combin type or External Piedmont Zone). UHP conditions are recorded in the Lago di Cignana unit (Groppo et al., 2009; Reinecke, 1998) in the upper Valtournenche valley. On the other hand, at the uppermost levels, the Chenaillet ophiolite lacks an Alpine metamorphic overprint (e.g. Lewis & Snewing, 1980; Manatschal et al., 2011; Mével et al., 1978).

Along the Susa and Chisone valleys transect (Fig. 1b; see Malusà et al., 2002 for a detailed review), crossing the here investigated area, eclogite-facies conditions are recorded to the east by the Internal Piedmont Zone (Ghignone et al., 2020; Pognante & Kienast, 1987), passing to the west to epidote-blueschist-facies conditions(Cerogne-Ciantiplagna unit of Polino et al.,

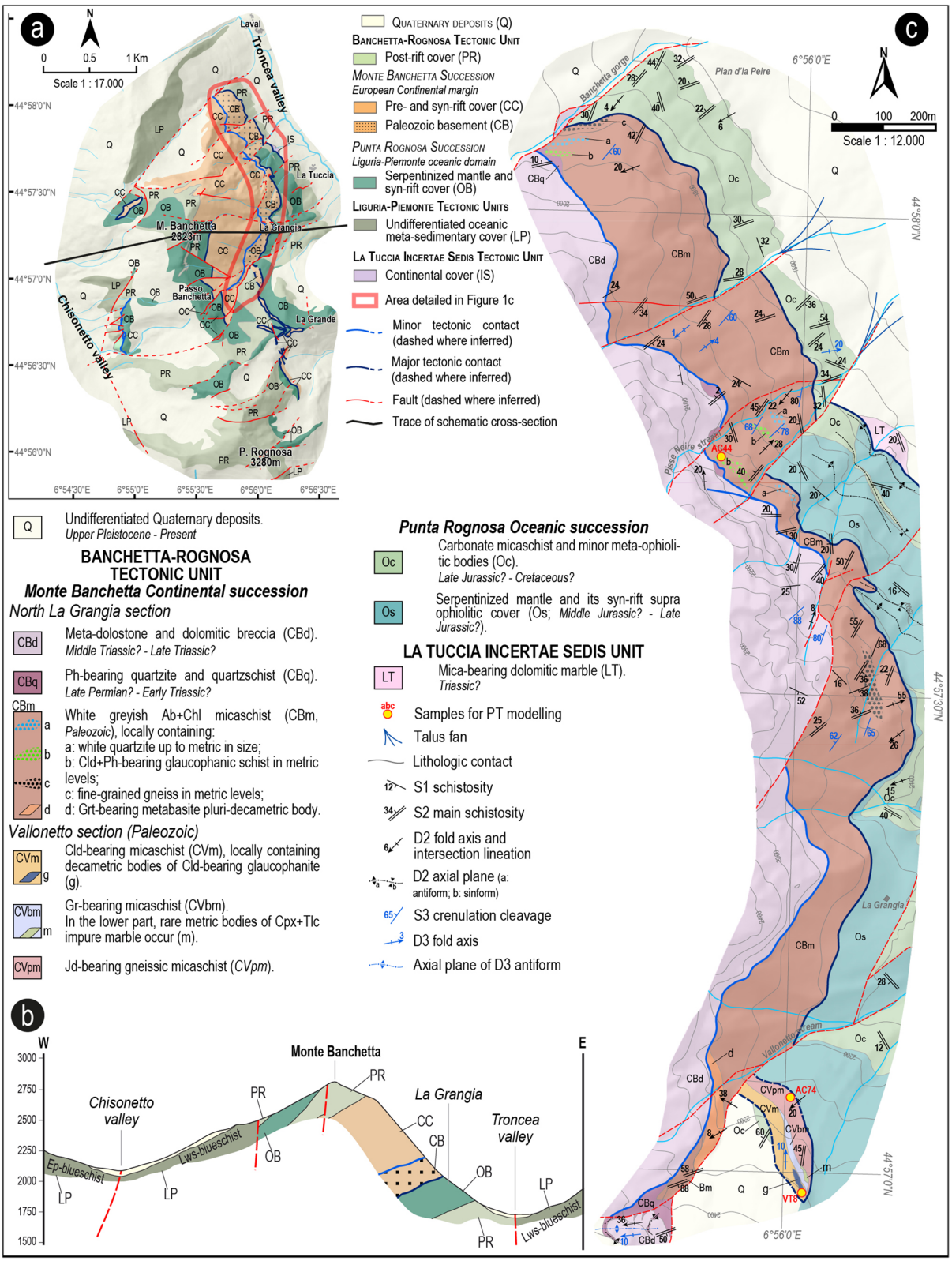

Fig. 2 **a** Tectonic sketch map of the Banchetta-Rognosa tectonic unit (modified from Corno et al., 2021); **b** Schematic cross-section of the Banchetta-Rognosa tectonic unit and neighboring units, lines and colors are according **a**; **c** Detailed geological map of the continental succession of the Banchetta-Rognosa tectonic unit, cropping out on the left side of Troncea valley, near Sestriere (Piemonte)

2002), and lawsonite-blueschist-facies conditions (i.e. Albergian and Lago Nero units of Agard et al., 2001; Giacometti & Rebay, 2013; Polino et al., 2002). The here investigated BRU is tectonically juxtaposed to these latter blueschist-facies units.

3 Geology of the Banchetta—Rognosa Unit (BRU)

3.1 General features and lithostratigraphy

The BRU crops out within an area of 10 km^2 on the mountain ridge between Troncea and Chisonetto valleys, where it is tectonically juxtaposed to several oceanic units (Servizio Geologico d'Italia, 2020; Fig. 2a, b). This unit consists of two successions respectively recording the Mesozoic tectono-depositional evolution of (i) a continental margin, i.e. Monte Banchetta succession, and (ii) a neighboring oceanic sector, i.e. Punta Rognosa succession. The continental and oceanic successions of the BRU are both covered by the same post-rift sediments consisting of Upper Jurassic?-Cretaceous carbonate micaschist. This peculiar architecture suggests pre-orogenic proximity (juxtaposition) of continental- and oceanic- derived rocks at the hyperextended European distal margin (Corno et al., 2021). Due to the occurrence of jadeite in the pre-Triassic basement and to the lithostratigraphic features of its overlying Mesozoic sedimentary cover, the continental part of the BRU has been correlated to the Acceglio-Col Longet nappe system (Caron, 1971; Caron & Saliot, 1969).

The Punta Rognosa oceanic succession (Corno et al., 2019), is made of exhumed serpentinized mantle overlain by syn-rift Middle-Upper? Jurassic polymictic meta-breccia (with both oceanic- and continental- derived clasts) and metasandstone bodies.

This study focuses on the Monte Banchetta continental succession (Fig. 2c), whose main features can be observed between the Banchetta gorge and the Vallonetto stream (hereafter named *North La Grangia section*; Fig. 3a) and to the south of the Vallonetto stream (hereafter named *Vallonetto section*; Fig. 3c).

In the *North La Grangia section*, the continental basement mainly consists of a white-greyish strongly foliated micaschist sequence (CBm in Fig. 3a) hosting layers and bodies of different lithologies. The medium- to fine-grained micaschist consists of quartz, white mica, chlorite, albite, epidote and graphite. The main lithological bodies embedded within the micaschist include: (i) chloritoid + phengite-bearing glaucophanic schist (b in Figs. 3a and 4), up to 2 m in thickness, mostly located in the central portion of the tectonic slice (see detailed petrographic description in Sect. 5.1); (ii) white quartzite layers (a in Fig. 3a), usually occurring in the upper portion of the micaschist; (iii) fine-grained gneiss (c in Fig. 3a), consisting of quartz, white mica, chlorite, albite widely occurring along the whole Banchetta eastern side, in decametric-thick levels; (iv) a pluri-decametric body of metabasite is exposed in the southernmost part of the *North La Grangia section* (d in Fig. 3a and b), including discontinuous white meta-aplites (1–2 m in length and up to 30 cm in thickness). This metabasite is a medium-grained massive rock consisting of glaucophane, garnet, chlorite, epidote, albite, titanite and minor paragonite, rutile, K-feldspar and quartz (Fig. 5a). The main foliation is defined by the alignment of glaucophane and epidote. Garnet porphyroblasts (up to 1 mm in diameter and pale yellow in color) occur in discontinuous domains wrapped by the main foliation. A sharp discontinuity in their composition suggests the existence of two different generations of garnet (Fig. 5b): a locally embayed Ca + Fe-rich core (Grt1), likely pre-Alpine in age, is surrounded by a Mn-rich Alpine rim (Grt2; see Additional file 1 for compositional diagrams). K-feldspar, interpreted as a relict phase, occurs in small crystals (up to 15 μm) in sub-mm patches with chlorite, epidote and rare muscovite (Fig. 5c).The whole micaschist sequence is unconformably covered by Upper Permian-Lower Triassic siliciclastic deposits (CBq in Fig. 3a), represented by white-greenish massive quartzite, locally micro-conglomeratic in the lower part (with detrital pink quartz clasts) and with phengite-bearing quartzite schists in the upper part. Upsection, Triassic meta-dolostone (up to 20–30 m-thick) and monomictic, clast-supported, meta-breccia occur (CBd in Fig. 2c). The dolomitic clasts of the meta-breccia are polycrystalline, up to few decimeters in size, and are set within a dolomitic matrix with sporadic decametric levels of black shale, carbonatic micaschist and phyllite. Then, the overlying syn-rift cover (up to 200 m

(See figure on next page.)

Fig. 3 **a** Lithostratigraphic succession of the *North La Grangia section*. Red polygon shows the location of the analyzed sample, used for P–T pseudosection modeling. Acronyms are: CBm, Ab + Chl micaschist; a, quartzite levels; b, Cld + Ph-bearing glaucophanic schist; c, fine-grained gneiss; d, metabasite body with meta-aplites (white bodies); CBq, Ph-bearing quartzite; **b** Field photograph of the metabasite body (d) within the Ab + Chl micaschist of the *North La Grangia section*. The main foliation (S1) is highlighted by whitish meta-aplites layers and is sub-parallel to primary lithological surface, S2 grows in axial plane of D2 folds; **c** Lithostratigraphic succession of the *Vallonetto* section. Red polygons show the location of analyzed samples, used for P–T pseudosection modeling. Acronyms are: CVpm, Jd-bearing gneissic micaschist; CVbm, Gr-bearing micaschist; m, Tlc + Aeg-bearing impure marble; CVm, Cld-bearing micaschist; g, Cld-bearing glaucophanite bodies; fg, fine-grained gneiss; dq, dark quartzites; **d** Field photograph of Jd-bearing gneissic micaschist of the *Vallonetto* section (modified from Corno et al., 2021); D2 folds transpose S1 compositional banding and develop S2 axial plane schistosity, D3 tectono-metamorphic event is expressed by S3 crenulation cleavage

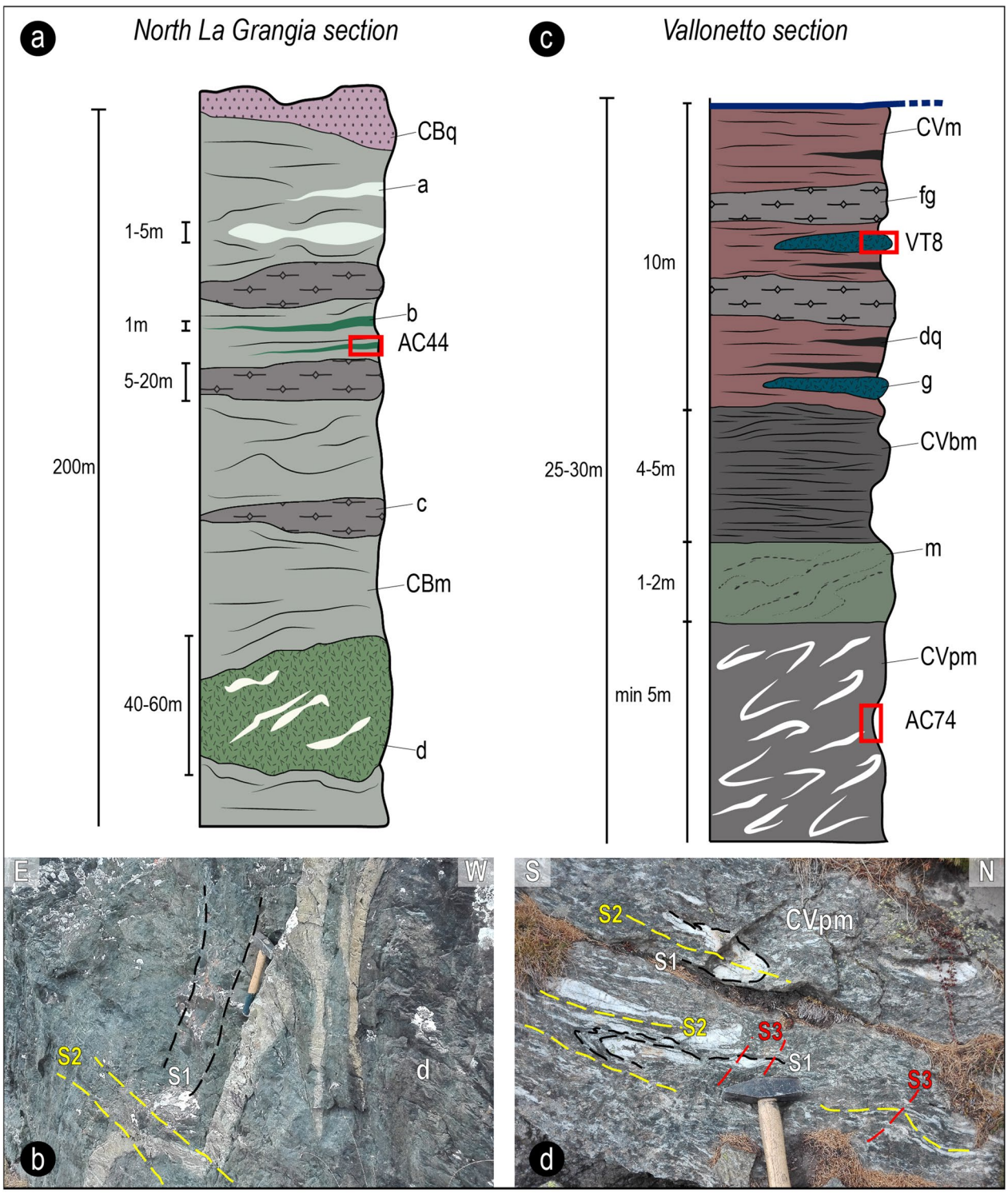

Fig. 3 (See legend on previous page.)

thick, see also Corno et al., 2021) consists of polymictic meta-breccia, black micaschist, and carbonate-bearing quartzite. The polymictic meta-breccia is composed of meta-dolostone and quartzite clasts in a carbonate matrix containing minor Cr-bearing white mica, talc and detrital K-feldspar. In the uppermost part of the

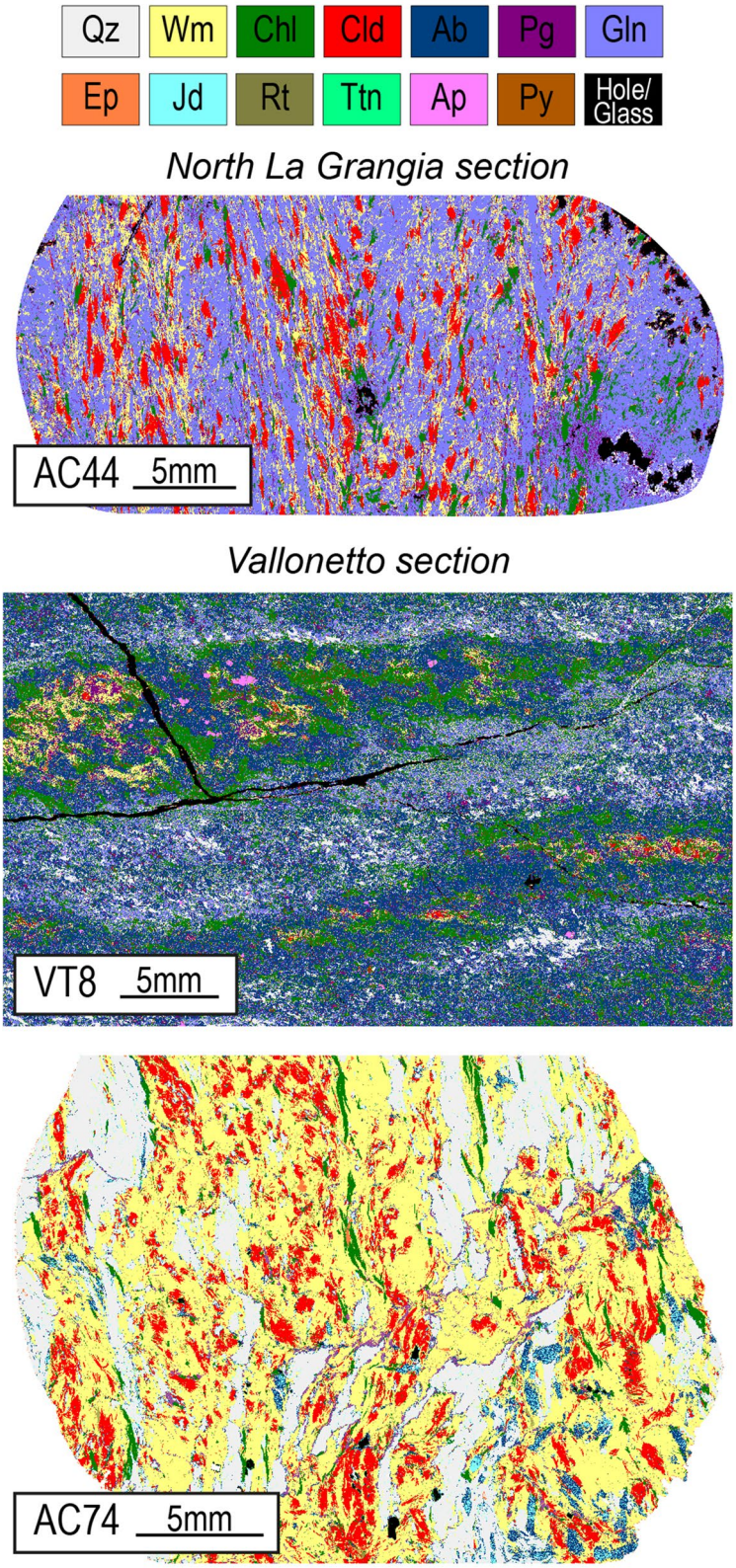

Fig. 4 Processed X-ray maps of the modelled samples from the *North La Grangia* and *Vallonetto* sections

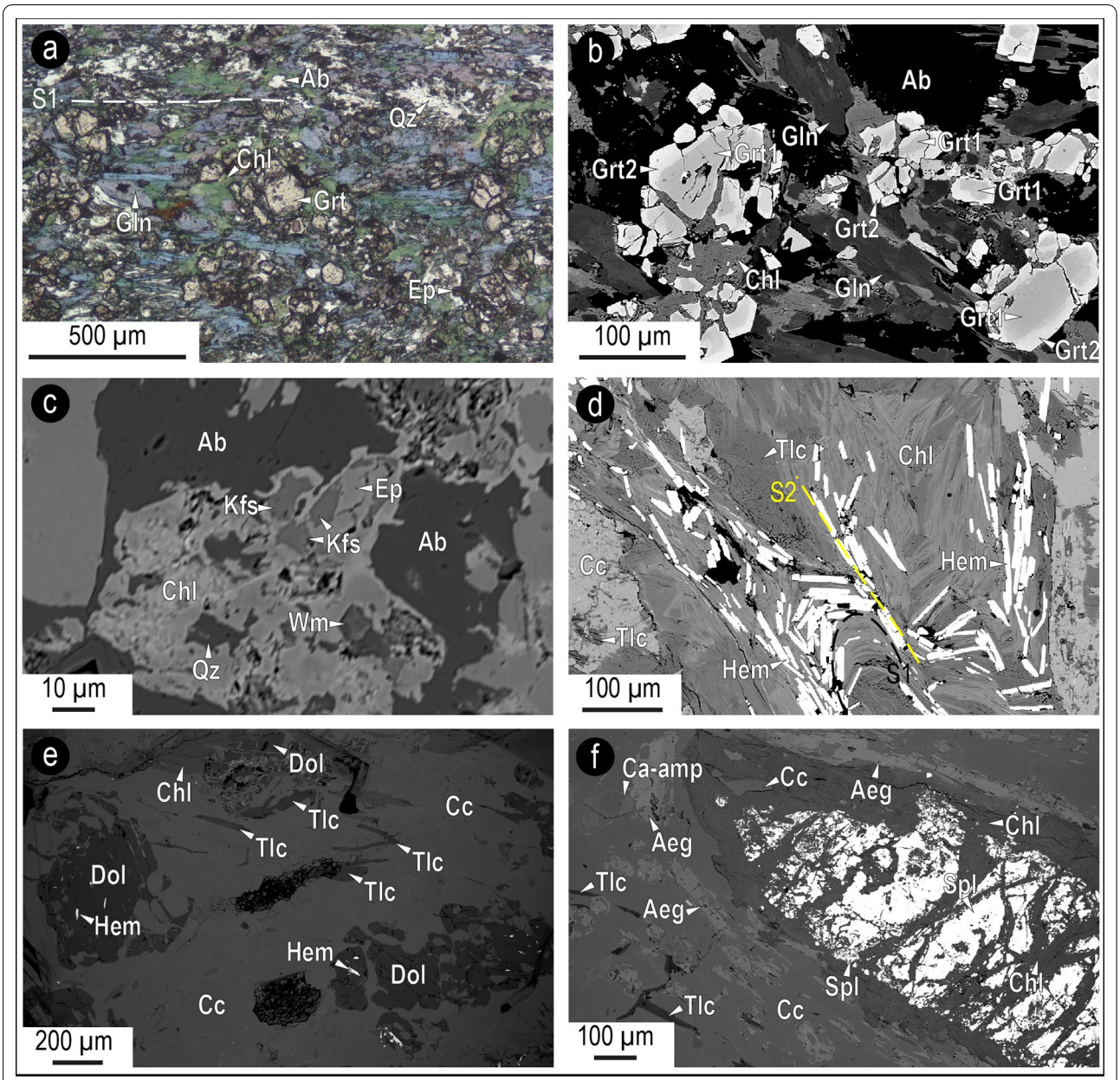

Fig. 5 Representative microstructures of the Monte Banchetta continental succession. (a, b, c) metabasite body. **a** Garnet porphyroblasts partially retrogressed to chlorite and wrapped by S1 foliation, defined by glaucophane + epidote + quartz, partially retrogressed to poikiloblastic albite (Plane Polarized Light, PPL); **b** Garnet porphyroblasts displaying an outer Mn-rich Alpine rim and an inner Ca + Fe-rich, likely pre-Alpine core (Back Scattered Electron image, BSE); **c** Detail on a sub-mm patch made of relict K-feldspar + epidote + chlorite + white mica (BSE). (d, e, f) Tlc + Aeg-bearing impure marble; **d** S1 hematite foliation transposed by S2 schistosity (BSE); **e** Calcitic matrix with relict crystals of dolomite + hematite and talc flakes oriented along the S1 foliation (BSE); **f** Large chromite crystals wrapped by chlorite, growing also along micro-fractures. Note aegirine partially retrogressed by Ca-amphiboles and talc flakes dispersed in the calcitic matrix (BSE)

polymictic meta-breccia, an impure quartzite contains meta-dolostone clasts up to decimetric in size.

The *Vallonetto section* identifies a tectonic slice (only a few hundred meters long and 30 m thick) of pre-Triassic basement rocks whose lower terms are made of dark grey jadeite-bearing gneissic micaschist (CVpm in Figs. 3c, d and 4). Locally, bodies (2–3 m in size) of medium- to coarse-grained impure marble occur above the gneissic micaschist (m in Fig. 2c). The marble consists of calcite, dolomite, talc, amphibole, epidote, aegirine, chlorite, hematite, and relict spinel. Due to the high oxygen fugacity in these marble bodies, all iron is ferric, stabilizing

hematite and aegirine (see Additional file 1). Due to the absence of ferrous iron, Mg-rich minerals like talc become stable. The matrix is mostly made of calcite while the main foliation is defined by discontinuous mm-thick layers of hematite + chlorite + talc (Fig. 5d). A second, poorly developed, foliation is defined by the oriented growth of large crystals of zoned Mg-riebeckite amphibole (up to 250 μm) + chlorite + epidote. Aegirine porphyroblasts, up to half a mm long, are wrapped by the main foliation and are concentrated in discontinuous domains, often in association with talc. Dolomite crystals, up to 300-400 μm in diameter, are dispersed in the matrix and are partially replaced by calcite. They often include hematite flakes and are partially enveloped by talc (Fig. 5e). Widespread through the rock, large relict crystals (up to 2 mm) of Cr-bearing spinel occur, wrapped by the main foliation (Fig. 5f). Late Ca-amphiboles overgrow talc and aegirine. Up section, a graphitic micaschist follows (CVbm in Fig. 3c), consisting of white micas (both phengite and muscovite), chlorite, albite, quartz, graphite and rare calcite. The tectonic slice ends upward with a ~ 10 m -thick reddish chloritoid-bearing micaschist (CVm in Fig. 3c), with local levels of fine-grained gneiss (consisting of white micas, quartz, chloritoid, chlorite, albite and allanitic epidote; fg in Fig. 3c) and dark quartzites (dq in Fig. 3c). Especially in the upper part, this chloritoid-bearing micaschist embeds minor metric bodies of chloritoid-bearing glaucophanites (g in Figs. 3c and 4).

3.2 Structural evolution

A polyphasic evolution is recorded in the BRU, characterized by the overprinting of HP (D1 and D2 phases) and LP-LT deformation events (D3 phase), followed by a late folding (D4 phase) (Corno et al., 2019, 2021).

The oldest D1 event is responsible for the development of the S1 schistosity sub-parallel to primary compositional surfaces (S0) (Fig. 3b). S1 schistosity is deformed and transposed during D2 event into tight to isoclinal folds, whose axial plane schistosity S2 is usually the most penetrative planar fabric in the BRU (Fig. 3d), defined by epidote + phengite/paragonite ± glaucophane ± chloritoid assemblage. S2 mainly dips to W-NW and contains a pervasive L2 stretching lineation. A non-cylindrical folding for the D2 event is suggested by NE-SW trending A2 fold axis, sub-parallel to the L2 stretching lineation. Major contacts between continental- and oceanic-derived successions, as well as their minor intra-succession tectonic contacts, were deformed since the earliest deformation events (D1-D2). D3 event is recorded by mesoscopic folds and crenulations (Fig. 3d) with sub-horizontal ENE-WSW-trending axes and axial planes usually dipping at high angle to SSE. Some rocks record an incipient S3 crenulation cleavage, widely associated with retrogression and development of LT-LP assemblages (chlorite + muscovite + albite ± stilpnomelane ± pumpellyite; Corno et al., 2019, 2021). The late D4 event is responsible for the development of gentle km-scale folds, generally displaying sub-horizontal N-S trending axes and high-angle dipping axial planes. Tectonic contacts recorded a late top-to-S-SW extensional reactivation.

4 Methods

4.1 Petrography and mineral chemistry

A Scanning Electron Microscope (JEOL JSM-IT300LV) equipped with an energy-dispersive X-ray spectrometer (EDX), with a SDD (a silicon drift detector from Oxford Instruments), hosted at the Earth Science Department of the University of Turin, was used for the determination of major elements. The experimental conditions include: accelerating voltage 15 kV, 1 nA probe current, counting time 50 s, process time 5 μs and working distance of 10 mm. The measurements were conducted in high vacuum conditions. The EDX acquired spectra were corrected and calibrated both in energy and in intensity thanks to measurements performed on cobalt standard introduced in the vacuum chamber with the samples (see Reed, 2005 and Goldstein et al., 2017). The Microanalysis Suite Oxford INCA Energy 300, that enables spectra visualization and elements recognition, was employed. This technique, with adequate counting statistics ($> 10^6$ cnts), allows to reach sensitivity of the order of 0.1 wt% and accuracy around 1%. A ZAF data reduction program was used for spectra quantification. The resulting full quantitative analyses were performed, using natural oxides and silicates from Astimex Scientific Limited®, as standards. All the analyses were recalculated using the MINSORT computer software (Petrakakis & Dietrich, 1985).

Potassic white micas have been classified as muscovite or phengite according to their Al_{tot}/Si ratio (i.e. muscovite: $Al_{tot} > 5.00$, $Si < 3.25$; phengite: $Al_{tot} < 5.00$, $Si > 3.25$). X_{Mg} of chloritoid, chlorite, amphiboles and white mica is defined as $Mg/(Mg + Fe^{2+})$. X_{Zo} in epidote is defined as $Al/(Al + Fe^{3+})$. Representative analyses of mineral composition are reported in the Additional file 1. Mineral abbreviations are according to Whitney and Evans (2010) (Wm = potassic white mica).

4.2 Phase diagram modeling

Isochemical phase diagrams (i.e. P–T pseudosections) were calculated for a Cld + Ph-bearing glaucophanic schist (sample AC44 in Fig. 3a) from the *North La Grangia section*, a Cld-bearing glaucophanite (sample VT8 in Fig. 3b) and a Jd-bearing gneissic micaschist (sample AC74 in Fig. 3c) from the *Vallonetto section*. Sample locations are

Table 1 Bulk compositions (mol%) of the modelled samples

	North La Grangia section	*Vallonetto section*	
	AC44	**VT8**	**AC74**
SiO_2	58.16	63.20	64.70
Al_2O_3	13.74	12.88	19.84
FeO	9.23	8.10	6.12
Fe_2O_3	0.52	0.90	0.11
MgO	11.00	7.68	2.00
MnO	0.24	–	0.06
Na_2O	5.60	6.41	3.82
K_2O	1.51	0.81	3.35
Total	100.00	99.98	100.00

reported in Figs. 2c, 3a and c. GPS coordinates of sampled locations are listed in the Additional file 1.

High-resolution multispectral maps of the thin sections used for deriving the effective bulk compositions of the investigated samples were obtained using the same SEM instrument, described in Sect. 4.1. Operative conditions used for mapping the entire thin sections were: 15 kV accelerating voltage, 5nA probe current, 1 µs EDS process time, 10^5 cnts/s, 2.5 µm point step, 1 ms dwell time. The row data were processed using the MultiSpec© software in order to obtain the modal compositions (vol% of all the minerals).

For each sample, the processed X-ray maps are reported in Fig. 3.

Bulk rock compositions of these samples (Table 1) were calculated by combining the mineral proportions obtained from the quantitative modal estimate of SEM–EDS multispectral maps with mineral chemistry acquired at SEM–EDS.

The isochemical phase diagrams were calculated in the system MnNKFMASOH (MnO-Na_2O-K_2O-FeO-MgO-Al_2O_3-SiO_2-O_2-H_2O) for samples AC44 and AC74 and in the system NKFMASOH (Na_2O-K_2O-FeO-MgO-Al_2O_3-SiO_2-O_2-H_2O) for sample VT8,using Perple_X 6.9.0 (Connolly, 1990, 2005, 2009), the internally consistent thermodynamic database of Holland and Powell (2011) (ds62) and the equation of state for H_2O of Holland and Powell (1998). Fluid saturated conditions were assumed, and the fluid was considered as pure H_2O ($aH_2O = 1$). This last assumption is realistic for the studied samples, because of the large occurrence of hydrous phases and the absence of primary carbonates and sulphides.

CaO was neglected in all pseudosections, because Ca-bearing phases are lacking. TiO_2 was not included in the calculation because rutile is the only Ti-bearing phase stable at HP conditions in all the samples.

The following solid solution models were used: biotite, chlorite, chloritoid, garnet, staurolite, white mica (White et al., 2014), clinopyroxene (Green et al., 2007), amphibole (Green et al., 2016), feldspar (Fuhrman & Lindsley, 1988), carpholite (Smye et al., 2010) and epidote (Holland & Powell, 1998). Quartz, lawsonite and kyanite were considered as pure phases.

5 Petrography and mineral chemistry of selected samples

Three samples have been selected from the pre-Triassic basement rocks of the Monte Banchetta succession out of a total of about 30 samples, based on their mineral assemblages, which are considered as the most suitable for constraining the HP tectono-metamorphic evolution of the BRU. Petrographic features and mineral chemical data are briefly summarized here for the three samples that have been selected for further petrological investigations: AC44 (Cld + Ph-bearing glaucophanic schist), VT8 (Cld-bearing glaucophanite) and AC74 (Jd-bearing gneissic micaschist). The blastesis-deformation relationships of the selected samples, as well as their mineral chemical data, are summarized in Tables 2 and 3, respectively.

5.1 *North La Grangia* section

5.1.1 Sample AC44: Cld + Ph-bearing glaucophanic schist

AC44 sample is a glaucophane + chloritoid- bearing schist, consisting of glaucophane (53%), chloritoid (11%), potassic white mica (18%), chlorite (9%), paragonite (7%) and rutile (2%). Its well-developed foliation (S2), defined by phengite, glaucophane, chloritoid and paragonite (Figs. 4 and 6a), is derived from the transposition of an earlier schistosity (S1; Figs. 6a-b), preserved as polygonal arcs and intrafolial folds, highlighted by chloritoid and glaucophane crystals besides phengitic and paragonitic micas. Chlorite occurs as a late phase, statically overgrowing chloritoid and glaucophane (Fig. 6b). Large flakes of muscovite statically overgrow S1- and S2-related phengite flakes.

Different white mica generations have different compositions, with highest Si content for phengite (Si from 3.30 up to 3.62 a.p.f.u.) and a strong decrease in Si content for the late muscovite flakes (Si < 3.25 a.p.f.u.) (Fig. 7a). Both syn-D1 and syn-D2 Na-amphiboles are glaucophane according to the classifications of Hawthorne et al. (2012) and Leake (1978) (Fig. 7b) and their X_{Mg} ranges from 0.56 to 0.67. Syn-D1 glaucophane crystals are usually zoned: lower X_{Mg} values (0.56–0.62) occur in prograde cores, while higher values (0.63–0.67) occur at peak syn-D1 rims. They generally display high Na(M4) values, close to theoretical value of 2.00 a.p.f.u. for glaucophane. Chloritoid of both generations (i.e. syn-D1 and syn-D2) has

Table 2 Blastesis-deformation relationships of selected samples

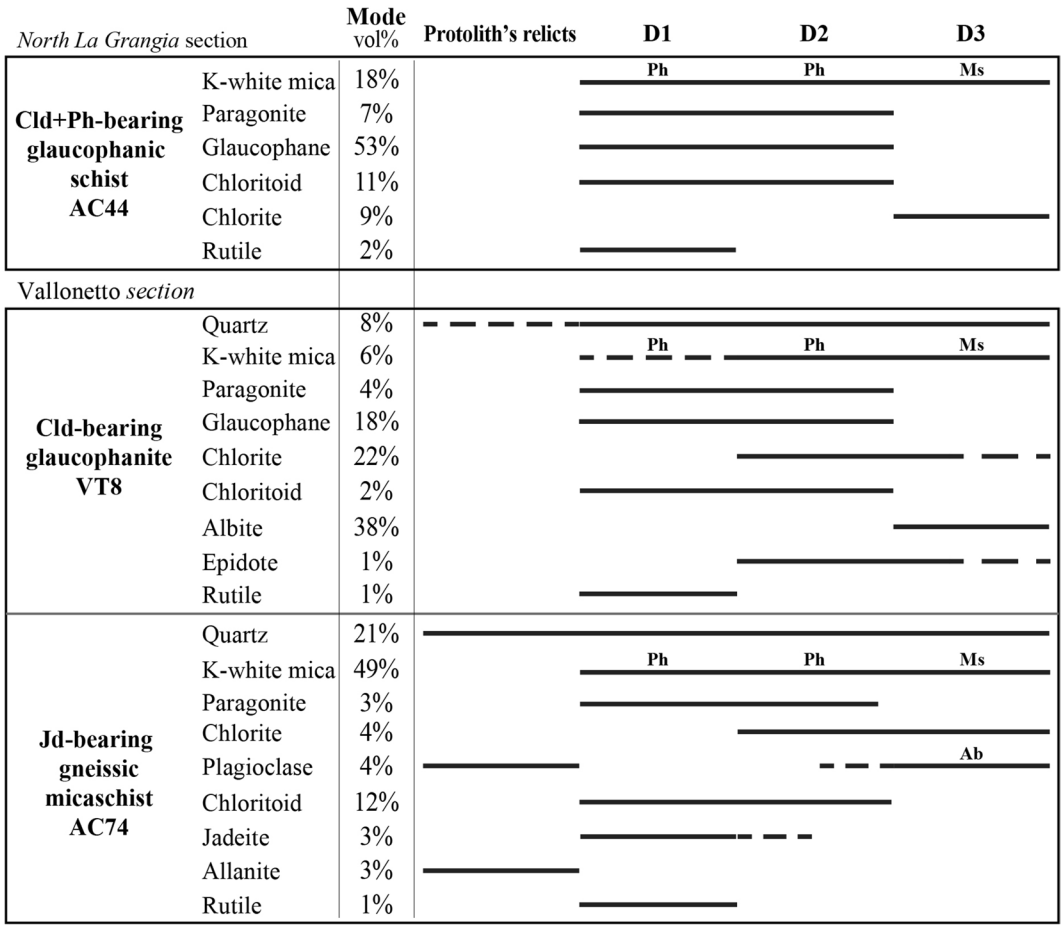

Table 3 Summary mineral compositions for the modelled samples

		North La Grangia section	*Vallonetto section*	
		AC44	VT8	AC74
Wm	Ph	Si = 3.40–3.62	Si = 3.29–3.38	Si = 3.32–3.56
	Ms	Si = 3.01–3.03	Si = 3.13–3.28	Si = 3.01–3.03
Pg		Na = 1.90–1.95	Na = 1.72–1.86	Na = 1.80–1.90
Gln		Na(B) = 1.96–2.00 Ca(B) = 0.00 X_{Mg} = 0.56–0.67	Na(B) = 1.96–2 Ca(B) = 0.00 X_{Mg} = 0.59–0.67	
Jd				X_{Acm} = 0.05–0.11
Cld		X_{Mg} = 0.15–0.18	X_{Mg} = 0.14–0.19	X_{Mg} = 0.13–0.14
Chl		X_{Mg} = 0.47–0.54	X_{Mg} = 0.43–0.58	X_{Mg} = 0.32–0.35

low X_{Mg}, in the range 0.15–0.18, and it locally contains low amounts of MnO, always lower than 2 wt%. Chlorite plots in the ripidolite field and has X_{Mg} between 0.47 and 0.54.

5.2 *Vallonetto* section

5.2.1 Sample VT8: Cld-bearing glaucophanite

This sample is a medium-grained, partially retrograded, glaucophanite consisting of chlorite (22%), glaucophane (18%), albite (38%), potassic white mica (6%), paragonite (4%), chloritoid (2%), quartz (8%), minor epidote (1%), and accessory rutile, zircon and apatite (~ 1% in total; Fig. 4). Chloritoid, potassic white mica and paragonite are concentrated in lens-like discontinuous domains, whereas quartz only occurs in the matrix (Figs. 4 and 6c). The main foliation (S2) is defined by the alignment of white micas, glaucophane, chlorite and chloritoid, and it is derived from the transposition of an older schistosity (S1) defined by the preferred orientation of an earlier generation of glaucophane and chloritoid (Fig. 6d), still preserved in mm–sized microlithons wrapped by the main foliation (S2). White mica occurs as phengite and paragonite (Fig. 6d), partially replaced by static growth of muscovite. Glaucophane crystals, up to 400 μm, are locally replaced at the rim by poikiloblastic albite or, along fractures, by fine-grained

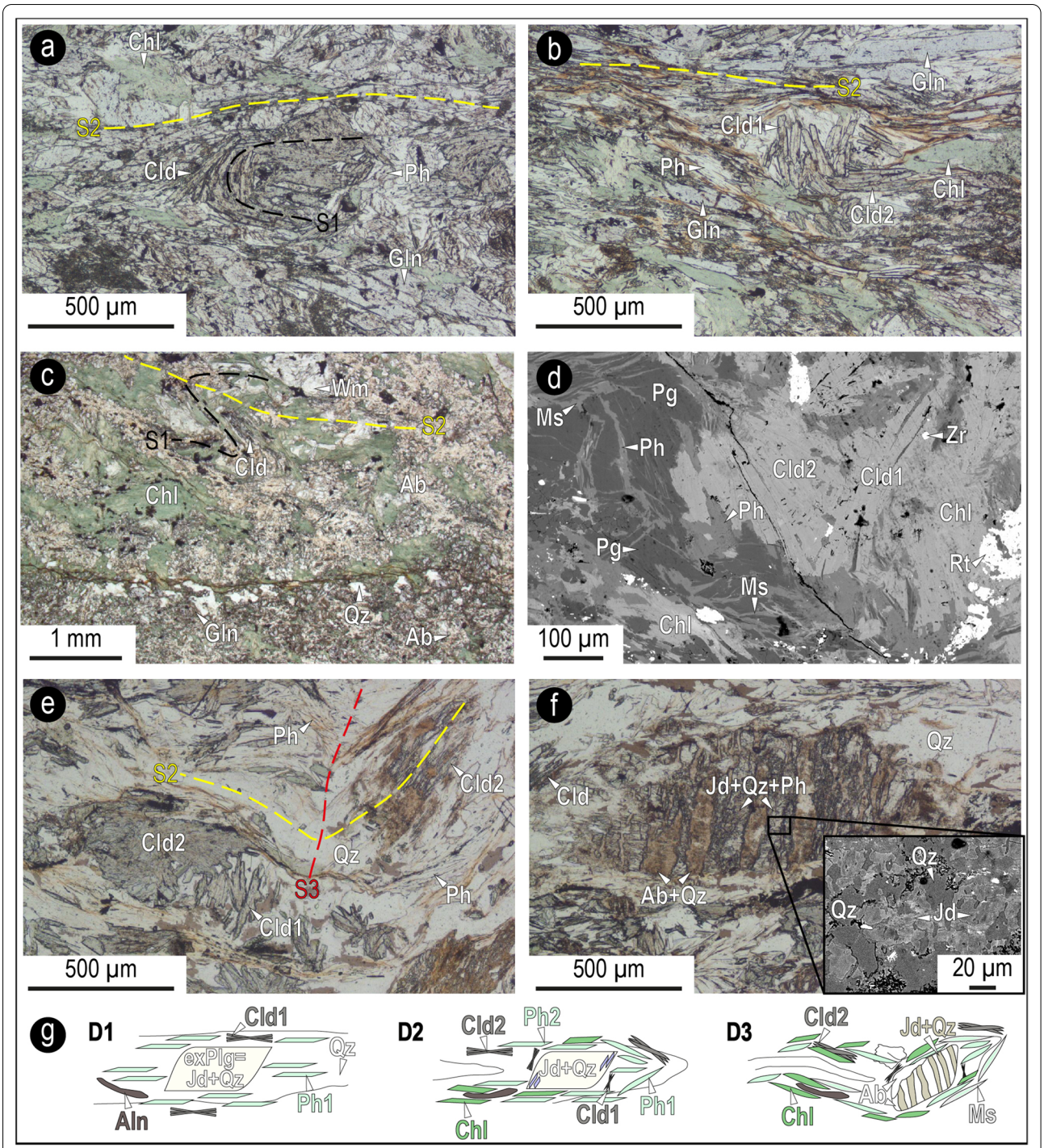

Fig. 6 Representative microstructures of the samples used for P–T modeling. **a**, **b** AC44. **a** Polygonal arc of chloritoid crystals, with S2 axial plane schistosity defined by phengite + glaucophane (PPL); **b** S1 microlithon with chloritoid crystals (Cld1) wrapped by S2 main foliation, defined by a second generation chloritoid (Cld2) + glaucophane + phengite. Chlorite replaces both chloritoid and glaucophane (PPL). **c**, **d** Sample VT8. **c** Boundary between matrix (lower part) and a lens-like domain (upper part), with relic S1 foliation almost completely replaced by white mica (= Wm) + chlorite + albite S2 axial plane schistosity (PPL); **d** Intergrowth of white mica and paragonite close to syn-D2 chloritoid crystals (Cld2), almost completely replacing syn-D1 chloritoid (Cld1); note on the right a large rutile crystal (BSE). **e**–**g** Sample AC74. **e** Syn-D1 chloritoid crystals (Cld1) preserved in a microlithon wrapped by S2 main foliation, defined by a second generation of chloritoid (Cld2) + phengite + quartz. Note the micro-scale expression of D3 tectono-metamorphic event, characterized by gentle folding (PPL); **f** Partially retrogressed syn-D1 jadeite crystal, wrapped by the main foliation and locally replaced by albite + quartz intergrowth (PPL). The inset shows a detail of jadeite + quartz intergrowth (BSE); **g** Schematic cartoon showing the most characteristic micro-structures and relationships of the three main tectono-metamorphic events

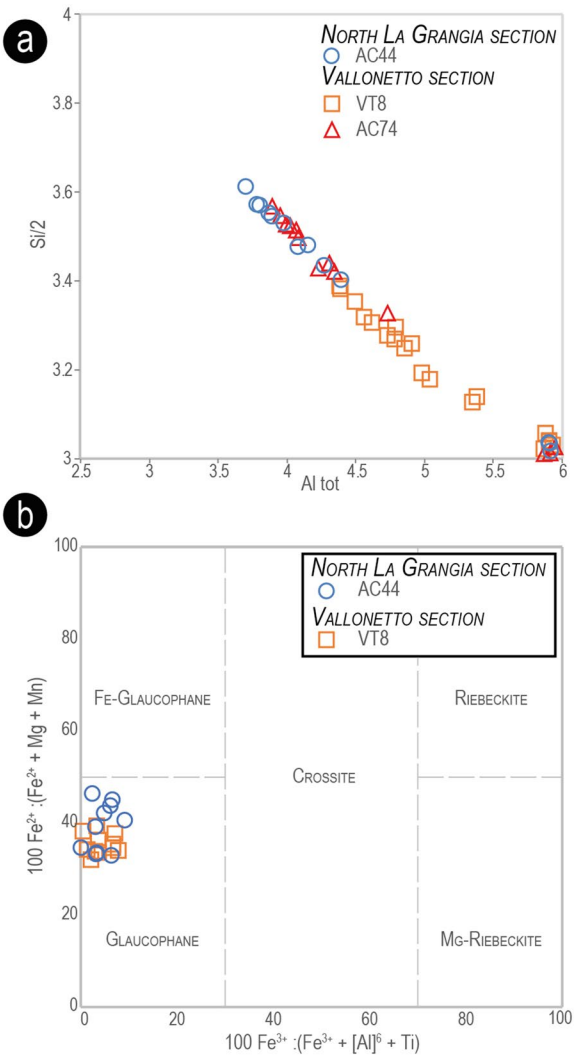

Fig. 7 Compositional diagrams for potassic white mica (**a**) and Na-amphibole (**b**) in the three selected samples

quartz + chlorite. Among accessory phases, abundant and large (up to 500 µm in length) rutile can be found together with zircon.

Phengite has Si content ranging from 3.30 to 3.40 a.p.f.u. and an X_{Mg} = 0.31–0.54; muscovite overgrowing phengite flakes has Si < 3.25 a.p.f.u. (Fig. 7a). Both syn-D1 and syn-D2 Na-amphiboles plot in the glaucophane field according to Hawthorne et al. (2012) and Leake (1978) classification criteria (Fig. 7b) and have X_{Mg} ranging from 0.59 to 0.67. Both generations of chloritoid (i.e. syn-D1 and syn-D2) have similar low X_{Mg} values in the range 0.14–0.19, and low MnO contents, always lower than 2 wt%. Chlorite plots in the ripidolite and picnochlorite fields and have X_{Mg} values between 0.45 and 0.54.

5.3 Sample AC74: Jd-bearing gneissic micaschist

This sample is a medium-grained gneissic micaschist consisting of quartz (21%), potassic white mica (49%), jadeite (3%), chloritoid (12%), chlorite (4%), albite (4%), paragonite (3%), and accessory allanite (3%) and rutile (1%). The main foliation (S2) is defined by the alignment of white micas, chlorite and chloritoid, concentrated in pluri-mm thick layers, alternated with discontinuous quartz-rich layers (Figs. 4 and 6e). A relic S1 foliation is defined by quartz + white micas + chloritoid + jadeite + rutile and is highlighted by polygonal arcs and intrafolial folds preserved within microlithons (Fig. 6e and f). Chloritoid occurs in two generations: an earlier syn-D1 generation, oriented at high angle with respect to the S2, and a syn-D2 generation (Fig. 6e and f). Jadeite porphyroblasts, up to 1.3 mm in size, are enveloped by the main foliation and are partially and variably retrogressed (Fig. 6f). The preserved portions of jadeite display intergrowth relationships with quartz and pre-kinematic white mica, while retrogressed portions are completely replaced by a fine-grained aggregate of quartz and albite. Late albite, chlorite and muscovite grow statically on the main foliation. Among accessory phases, mm-sized relicts of allanite are wrapped by the main foliation and include zircon and monazite. A schematic metamorphic evolution through the three main tectono-metamorphic event is reported in Fig. 6g.

White mica occurs as potassic white mica and paragonite. Phengite and paragonite are related to D1 and D2 tectono-metamorphic events, and are partially replaced by static growth of syn-D3 muscovite. Phengite flakes have the highest Si contents (Si from 3.30 up to 3.56 a.p.f.u; Fig. 7a). X_{Mg} in phengite ranges between 0.48 and 0.75. Na-pyroxene is almost a pure jadeite according to Morimoto (1988), with Acmite < 15% (see Additional file 1). Both chloritoid generations (i.e. syn-D1 and syn-D2) have low X_{Mg} values of 0.13–0.14, and low MnO contents, always lower than 1 wt%. Chlorite plots in the clinochlore field and has X_{Mg} ranging between 0.32 and 0.35.

6 Thermodynamic modeling

The peak P–T conditions of the selected samples were constrained using the isochemical phase diagram approach, based on the predicted stability field of the observed assemblages, combined with the intersection of compositional isopleths modelled for chloritoid and glaucophane (samples AC44 and VT8). Phengite compositional isopleths have not been used, due to the difficulties in assigning each composition to a specific phengite generation (syn-D1 or syn-D2). The general topology of

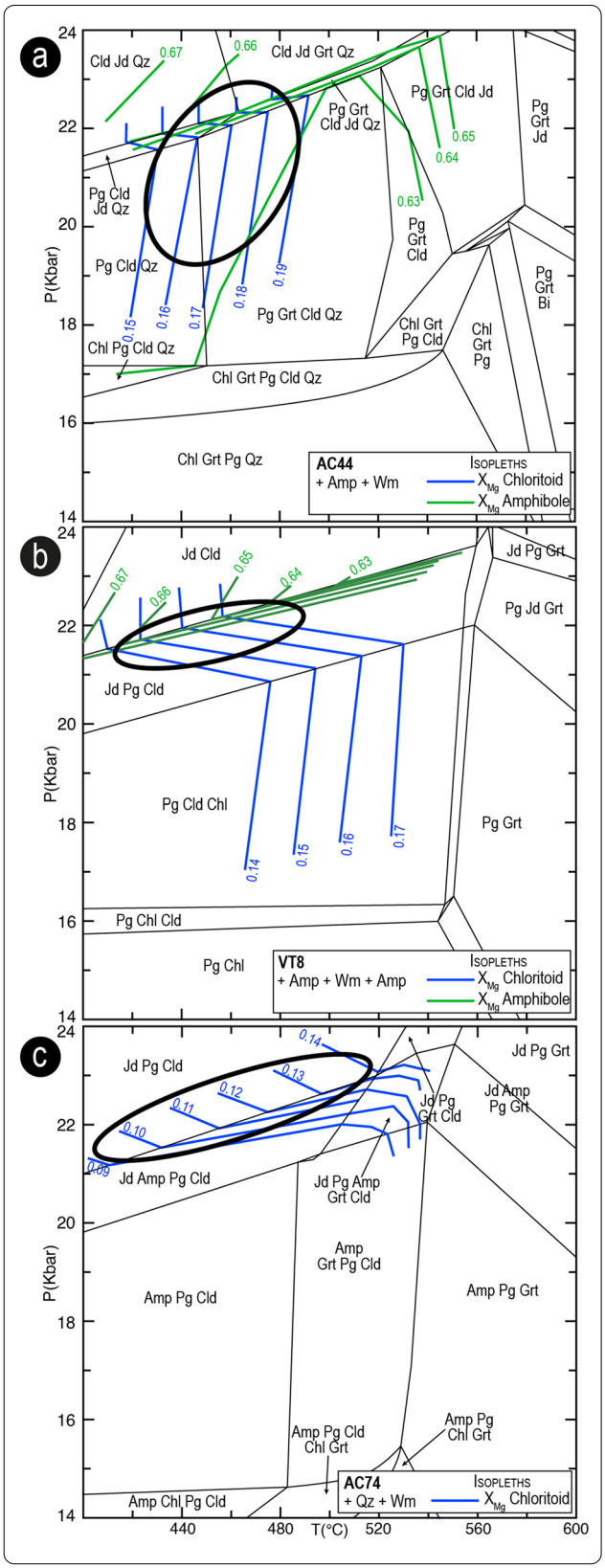

Fig. 8 P–T pseudosections modelled for the selected samples from the *North La Grangia* and the *Vallonetto* sections using the measured bulk compositions of samples **a** AC44, **b** VT8 and **c** AC74. The black ellipses show the constrained P–T conditions, based on the mineral assemblages and the intersection of compositional isopleths, as indicated in each legend. For clearness, all fields have been left white. Fields with five phases are quini-variant and those with six phases are quadri-variant, in all the pseudosections

the calculated phase diagram sections is similar for all the samples: chloritoid is predicted to be stable up to 530–560 °C and garnet appears in the temperature interval of 480–530 °C, depending on samples. Glaucophane and paragonite are predicted to be stable in almost the whole P–T region of interest; exceptions are for sample AC74, where glaucophane is limited to $P < 21–23$ kbar and for sample AC44, where paragonite is absent in the P–T range of 400–520 °C, 17.5–24 kbar.

6.1 *North La Grangia* section

6.1.1 Sample AC44

The modelled pseudosection is dominated mainly by quadri- and quini-variant fields (Fig. 8a). The observed peak assemblage (Gln + Cld + Ph + Pg + Qz) is modelled at $T < 450$ °C and $P = 17–22$ kbar; at $T > 450$ °C, garnet is predicted to occur in addition to these phases, whereas at $P > 21–22$ Kbar, jadeite appears at the expenses of paragonite. The modelled chloritoid and glaucophane compositional isopleths allow further constraining the peak P–T conditions for this sample. The X_{Mg} measured in chloritoid ($X_{Mg} = 0.15–0.18$) defines a T range of 420–480 °C, whereas the X_{Mg} measured in the syn-D1 glaucophane ($X_{Mg} = 0.63–0.67$) constrains pressure at 21–22 kbar, mostly in the narrow field where jadeite (< 0.15 vol%) coexists with paragonite. Very low modal amounts of garnet (< 1 vol%) are predicted to occur at these P–T conditions, although it has not been observed in the sample. Such low modal amount of garnet could have been likely replaced by retrograde chlorite, which is widespread in the sample. Similarly, quartz is not observed in the sample but the modelled pseudosection predicts its stability over a wide P–T range. In this case, the predicted modal amount of quartz is extremely low (< 0.2 vol%), and quartz could have been easily overlooked. Overall, peak P–T conditions of 21–22 kbar and 450 ± 25 °C are constrained for this sample.

6.2 *Vallonetto* section

6.2.1 Sample VT8

The modelled pseudosection consists of large quadri-variant fields and smaller tri-variant fields (Fig. 8b). The observed peak assemblage (Qz + Ph + Pg + Cld + Gln)

is predicted to be stable in a large field ranging from 16 to 20–22 kbar and at T < 530 °C, limited by the garnet appearance at T > 530 °C. At pressures higher than 20–22 kbar (depending on temperature), jadeite becomes stable together with paragonite; this last disappears at P > 22–23 kbar. The modeled compositional isopleths of chloritoid corresponding to its measured composition (X_{Mg} = 0.14–0.17) are nearly vertical in the jadeite-absent field, where they constrain temperatures in the range 460–520 °C; however, in the paragonite + jadeite field, the chloritoid isopleths become P-dependent and constrain P in the interval 21–22 kbar (for T = 420–520 °C). The X_{Mg} isopleths modeled for glaucophane and corresponding to its measured composition (X_{Mg} = 0.59–0.67) are concentrated in the paragonite + jadeite field and constrain P at 21–23 kbar. The intersection between chloritoid and glaucophane compositional isopleths further constrain peak P–T conditions at 450 ± 20 °C and 21–22.5 kbar, in the Qz + Ph + Pg + Cld + Gln + Jd field. The amount of jadeite predicted at peak P–T conditions is about 15–17 vol%; although jadeite is not preserved, its former occurrence in the HP assemblage is compatible with the high amounts of retrograde albite (38 vol%) observed in the sample.

6.3 Sample AC74

The modelled pseudosection is characterized mainly by quadri- and quini-variant fields (Fig. 8c). The observed peak assemblage (Qz + Jd + Ph + Pg + Cld) is predicted by a three-variant field at P > 22 kbar and T < 480–520 °C, limited toward lower pressures by the appearance of glaucophane, and toward higher temperatures by the appearance of garnet. The modelled compositional isopleths of chloritoid corresponding to its measured composition (X_{Mg} = 0.09–0.14) plot both in this field and in the nearby glaucophane-bearing field (Jd + Gln + Pg + Cld + Qz + Ph), in which low modal amounts of glaucophane (< 8 vol%) are predicted to occur. The former occurrence of low amounts of glaucophane in the peak assemblage, now completely replaced by retrograde chlorite + albite, cannot be excluded. Therefore, peak P–T conditions have been estimated at 21–23 kbar, 470 ± 50 °C, at the boundary between glaucophane-absent and glaucophane-bearing fields.

7 Discussion

7.1 What the basement rocks of the BRU tell us: from the protoliths to eclogite-facies metamorphism

The detailed lithostratigraphic, structural, petrographic and petrologic analysis of the poorly investigated basement rocks of the BRU allowed us to make some hypothesis about the nature of their protoliths and to reconstruct their metamorphic evolution.

7.2 Protoliths

The *North La Grangia section* can be interpreted as a heterogeneous and composite Paleozoic basement derived from an original sedimentary sequence, mostly consisting of intercalated pelites with different content and types of clay minerals (now transformed in Ab + Chl micaschist or Cld + Ph-bearing glaucophanic schist) intercalated with arenaceous pelites (now fine-grained gneiss), and of minor quartz-arenite (now quartzite), with the arenaceous fraction increasing upward. In this setting, the photolith of the metabasite body embedded in this sedimentary sequence can be interpreted as a pre-Alpine metamorphic rock derived from a mafic protolith, either of magmatic or of sedimentary origin. The occurrence of relicts of unzoned garnet cores and of few relict K-feldspars, suggests that relatively high-T conditions were reached during the pre-Alpine metamorphic event. In this framework, the observed abrupt Mn-enrichment in garnet rims could be interpreted as the onset of high-P overgrowth on a pre-existent pre-Alpine HT garnet, as reported in other units of the Alps in similar tectonic positions (Bucher et al., 2019),

The lower part of the *Vallonetto section* is made of Jd-bearing gneissic micaschist, followed upsection by a dark grey graphitic micaschist. At the contact between these two lithologies, discontinuous metric bodies of Tlc + Aeg-bearing impure marble locally occur. We suppose a magmatic protolith for the Jd-bearing gneissic micaschist, whereas the dark grey graphitic micaschist likely derived from an original sedimentary sequence mostly consisting of pelite ± rich in organic matter. The uppermost part of the *Vallonetto section* is made of Cld-bearing micaschist with detrital allanite and metric bodies of glaucophanite, suggesting a volcano-clastic origin for this sequence.

Both sequences containing some intrusive bodies were involved in the Alpine subduction and in the following exhumation, preserving their original lithostratigraphic configuration in spite of the intense deformation and metamorphic re-equilibration.

7.3 Alpine evolution

The Alpine tectono-metamorphic evolution of the Monte Banchetta succession of the BRU was reconstructed by applying the isochemical phase diagram modeling approach. The P–T path from peak conditions to the final exhumation was constrained, and related to the different deformation stages recognized in the study area.

The D1 tectono-metamorphic event – defined by phengite + paragonite + glaucophane I + chloritoid I + epidote I assemblage – occurred at the metamorphic peak, which has been constrained at 20–23 kbar and 440–500 °C. These peak P–T conditions have been constrained on

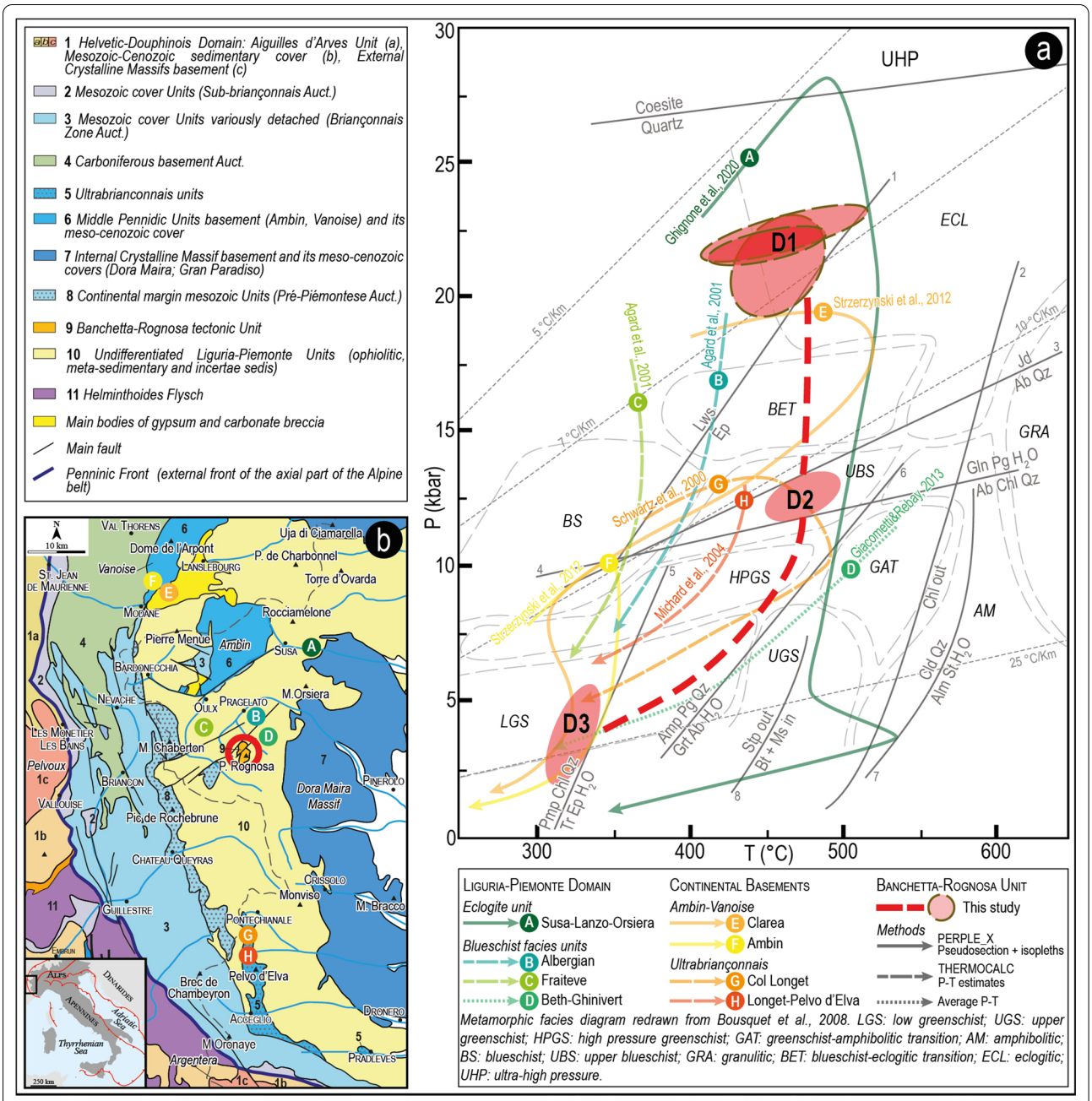

Fig. 9 **a** Compilation of P–T trajectories of different units of the Western Alps for comparison with the studied area. Whereas the D1 P–T estimates for the Banchetta-Rognosa unit were obtained by isochemical phase diagram modelling, the retrograde tectono-metamorphic events (i.e. D2 and D3) have been qualitatively inferred on the basis of mineral assemblages only. Different line patterns indicate different thermobarometric methods as reported in the legend. Reactions 1 to 8 are from: 1–2: Poli & Schmidt, 1995; 3: Holland, 1980; 4: Guiraud et al., 1990; 5: Evans, 1990; 6: Powell & Holland, 1990; 7: Rao & Johannes, 1979; 8: Nitsch, 1971; **b** Simplified tectonic map of the Western Alps (redrawn from the Structural Model of Italy, Bigi et al., 1990) and approximate location of units considered for comparison

the basis of the overlap of the P–T conditions (ellipses) inferred from the three modelled samples (Figs. 8 and 9). During the D1 event, jadeite developed in magmatic bodies with felsic composition of the *Vallonetto Section*. These peak P–T conditions are remarkably consistent among the investigated samples, which are representative of different chemical systems, and point to peak metamorphism within the eclogite-facies field (Fig. 9).

Based on minero-chemical composition of the metamorphic phases, similar P–T conditions (470–520 °C, at

17–19 Kbar) were inferred for the oceanic succession of the Monte Banchetta-Punta Rognosa unit (Corno et al., 2019). These data suggest a common metamorphic evolution for the oceanic and continental successions of the BRU, in agreement with the reconstructed tectono-stratigraphy and implying their pre-orogenic juxtaposition.

The D2 tectono-metamorphic event is testified by the development of the main foliation at the regional scale, defined by upper blueschist-facies assemblages: phengite ± paragonite + glaucophane II + chloritoid II + epidote II ± chlorite, and by the replacement of jadeite by albite + quartz in the gneissic micaschist of the *Vallonetto section* (sample AC74). Considering the reaction curves limiting the stability fields of the D2 assemblage (i.e. reactions 4 and 6 in Fig. 9), this event is qualitatively constrained at around 11–13 kbar and 450–500 °C. The D3 tectono-metamorphic event was responsible for the widespread retrogression of the HP mineral assemblages and the development of greenschist-facies assemblages (chlorite + albite + muscovite). Taking into account the fact that the oceanic succession of the BRU is tectonically juxtaposed with the continental succession since the first deformation stages, it is possible to suppose a common D3 event in the pumpellyite and stilpnomelane stability fields at about 350 °C and P < 5–7 kbar (Corno et al., 2019).

The exhumation path is characterized by an early decompression of at least 10 kbar, which was either isothermal or associated to a little T decrease, during which the Jd-out decompressional reaction was crossed, leading to the development of the main regional foliation (D2 event). This event developed in the glaucophane + paragonite stability field according to the reaction 4 in Fig. 9 and at lower T with respect to the amphibole + paragonite out/ garnet + albite in (reaction 6 in Fig. 9). Therefore, the S2 foliation was equilibrated at an apparent geothermal gradient of about 10–12 °C/km, corresponding to the upper blueschist-facies (UBS), and this suggests a subduction channel environment. The subsequent exhumation stage is marked by a further decompression of almost 7–8 kbar associated with a significant temperature decrease (cooling down to 350–400 °C), in the pumpellyite and stilpnomelane stability fields: this implies an increase in the geothermal gradient to ~ 25 °C/km, compatible with continental collision regime (D3 event).

7.4 Comparison between the BRU and neighboring units

In the investigated sector of the Alpine chain, both eclogitic and blueschist-facies units are exposed (see Malusà et al., 2002, and Agard, 2021, for a detailed review). Six of these units have been selected for a comparison with the BRU (Fig. 9 for locations of each unit), due to their proximity to the BRU and because their P–T paths have been already constrained in the literature. The selected units include: (i) the eclogite-facies, oceanic derived, Susa-Lanzo-Orsiera unit (Zermatt-Saas type; Servizio Geologico d'Italia, 2002) exposed in the Susa Valley (location A in Fig. 9b), the blueschist-facies, oceanic units exposed in (ii) the Beth-Ghinivert area, (iii) the Albergian area, (iv) the Fraiteve area (locations B, C and D in Fig. 9b), and the blueschist-facies, continental units exposed in (v) the Ambin-Vanoise Massif, and (vi) the Acceglio-Col Longet nappe (locations E–F and G-H in Fig. 9b). It is important to note that the P–T evolution of these units were constrained with different methods, ranging from the pseudosection approach (i.e. for the Susa-Lanzo-Orsiera unit and the Ambin-Vanoise Massif), to multi-equilibrium thermobarometry (average P–T method of THERMOCALC; Holland & Powell, 1998) (i.e. for the Beth-Ghinivert, Albergian and Fraiteve area), to conventional thermobarometry and/or the analysis of the position of relevant reactions in the P–T space (i.e. for the Albergian and Fraiteve zones and the Acceglio-Col Longet nappe).

For the oceanic-derived, eclogitic rocks of the Susa-Lanzo-Orsiera unit (i.e. the Internal Piedmont Zone), exposed in the Susa Valley (A in Fig. 9a), Ghignone et al. (2020) estimated peak P–T conditions of 25–29 kbar, 460–510 °C. The observed peak assemblages in metapelites include chloritoid + garnet + phengite + lawsonite, whereas those observed in metabasic rocks consist of garnet + omphacite + glaucophane + phengite + minor talc ± lawsonite.

The oceanic-derived blueschist units (i.e. External Piedmont Zone) exposed in the proximity of the BRU registered different peak P–T conditions, ranging from the greenschist-amphibolite-facies transition to the blueschist-eclogite-facies transition. In the Beth-Ghinivert area (D in Fig. 9a, just a few kilometers to the east from the BRU), Giacometti and Rebay (2013) estimated peak P–T conditions of 10 kbar, 492 ± 35 °C (peak assemblage in metapelites: phengite + chloritoid + chlorite ± epidote ± lawsonite; peak assemblage in metabasic rocks: Na-amphiboles + phengite + epidote ± chlorite). In the Albergian area (B in Fig. 9a, 5–7 kilometers to the North-East with respect to the BRU), Agard et al. (2001) estimated peak P–T conditions of 18–21 kbar, 390–450 °C (peak assemblage in metapelites: carpholite + chloritoid + phengite + paragonite + chlorite ± lawsonite; peak assemblage in metabasic rocks: phengite + paragonite + chlorite + glaucophane ± lawsonite). For the Fraiteve area (C in Fig. 9a, 5–7 kilometers to the North-West with respect to the BRU), the same authors estimated peak P–T conditions of 16.5–18.5

kbar, 300–390 °C (peak assemblage in metapelites: carpholite ± chloritoid + phengite + paragonite + chlorite + lawsonite; peak assemblage in metabasic rocks: glaucophane + epidote + chlorite + lawsonite).

Peak P–T conditions registered by the continental-derived, blueschist-facies units adjacent to the BRU are also variable. In the Ambin-Vanoise massif, Strzerzynski et al. (2012) estimated minimum eclogite-facies peak P–T conditions of 17.5 kbar, 470° C for the Clarea Unit (E in Fig. 9a) (peak assemblage: glaucophane + garnet + paragonite + phengite) and blueschist-facies conditions of 6.5–9 kbar, 350° C for the Ambin Unit (F in Fig. 9a) (peak assemblage: chlorite + phengite). In the Acceglio-Col Longet nappe, Schwartz et al. (2000) (G in Fig. 9a) and Michard et al. (2004) (H in Fig. 9a) estimated average P–T peak conditions of about 12–15 kbar, 400–450 °C (peak assemblage: quartz + jadeite + garnet + phengite + zoisite + paragonite + glaucophane) at the blueschist-eclogite-facies transition.

From this comparison, it appears that the BRU experienced a metamorphic peak within the eclogite-facies field, at P–T conditions intermediate between those registered by the eclogite-facies of the Internal Piedmont Zone (Ghignone et al., 2020) and those registered by the oceanic and continental-derived units classically ascribed to the blueschist-facies metamorphic domain. Our results thus suggest that the BRU could be one of the westernmost eclogite-facies unit in the Western Alps, therefore extending the eclogite-facies metamorphic domain toward the west. Although in the literature a correspondence between the continental-derived rocks of BRU and those of the Col Longet nappe (Ultrabriançonnais domain) has been proposed (Caron, 1971; Caron & Saliot, 1969), the two continental units recorded significantly different peak P–T conditions: the BRU registered peak pressures 12–15 kbar higher than those of the Col Longet nappe. The difference in peak P–T conditions is less marked between the BRU and the neighboring oceanic-derived units of the Beth-Ghinivert and Albergian-Fraiteve area; in this context a re-evaluation of their metamorphic evolution using the isochemical phase diagram approach is advisable, in order to test whether the apparent different peak metamorphic conditions could be imputable to different thermobarometric approaches.

Supplementary Information

The online version contains supplementary material available at https://doi.org/10.1186/s00015-021-00393-7.

Additional file 1. Representative analyses, samples location and supplementary diagrams.

Acknowledgements
We wish to thank Gianreto Manatschal, Luca Barale and Nicolò Incerpi for the discussion on the topics of present paper. We also wish to thank Domenico Rosselli of the Parchi Alpi Cozie for his support in the logistic during field work. The constructive comments of K. Bucher and an anonymous reviewer significantly improved this paper. We are thankful to E. Gnos for his editorial job. This work was financially supported by Ministero dell'Università e della Ricerca Scientifica e Tecnologica (M.I.U.R.).

Authors' contributions
Field work: AC, PM, GM; conceptualization: AC, PM, CG, AB and MG; data collection: AC, PM and AB; data analysis: AC and CG; thermodynamic modeling: CG, AC and AB; writing original draft: AC, CG, PM and AB; figures draft and editing: AC; validation: AC, PM, CG, MG and AB; writing, review and editing: AC, CG, PM, MG and AB. All authors read and approved the final manuscript.

Funding
This research was funded by research Grants from University of Torino, Ricerca Locale "ex 60%" (A.B., A.C. and M.G.).

Availability of data and materials
The datasets used and analyzed during the current study are available from the corresponding author on reasonable request. Representative analyses for the main minerals occurring in the 3 samples used for thermodynamic modeling are reported in the Additional file 1.

Declarations

Ethics approval and consent to participate
Not applicable.

Consent for publication
All authors gave consent for publication on the Swiss Journal of Geosciences.

Competing interests
The authors declare that they have no competing interests.

Author details
[1]Dipartimento Di Scienze Della Terra, Università Degli Studi Di Torino, Torino, Italia. [2]Istituto Di Geoscienze E Georisorse, CNR, Torino, Italia.

Received: 14 April 2021 Accepted: 12 July 2021
Published online: 16 September 2021

References

Agard, P. (2021). Subduction of oceanic lithosphere in the Alps: Selective and archetypal from (slow-spreading) oceans. *Earth-Science Reviews*, 103517.
Agard, P., Vidal, O., & Goffé, B. (2001). Interlayer and Si content of phengite in HP–LT carpholite-bearing metapelites. *Journal of Metamorphic Geology, 19*(5), 479–495.
Agard, P., Yamato, P., Jolivet, L., & Burov, E. (2009). Exhumation of oceanic blueschists and eclogites in subduction zones: Timing and mechanisms. *Earth-Science Reviews, 92*(1–2), 53–79.
Balestro, G., Festa, A., & Dilek, Y. (2019). Structural architecture of the Western Alpine Ophiolites, and the Jurassic seafloor spreading tectonics of the Alpine Tethys. *Journal of the Geological Society, 176*(5), 913–930.
Ballèvre, M., Camonin, A., Manzotti, P., & Poujol, M. (2020). A step towards unraveling the paleogeographic attribution of pre-Mesozoic basement complexes in the Western Alps based on U-Pb geochronology of Permian magmatism. *Swiss Journal of Geosciences, 113*, 1–28.
Bearth, P. (1967). Die Ophiolithe der Zone von Zermatt-Saas Fee. *Beiträge zur Geologischen Karte der Schweiz, Neue Folge*, p. 130.
Beltrando, M., Compagnoni, R., & Lombardo, B. (2010). (Ultra-) High-pressure metamorphism and orogenesis: An Alpine perspective. *Gondwana Reserch, 18*, 147–166.
Beltrando, M., Manatschal, G., Mohn, G., Dal Piaz, G. V., Vitale Brovarone, A., & Masini, E. (2014). Recognizing remnants of magma-poor rifted margins

in high-pressure orogenic belts: The Alpine case study. *Earth-Science Reviews, 131*, 88–115.
Bigi, G., Castellarin, A., Coli, M., Dal Piaz, G.V., Sartori, R., Scandone, P. & Vai, G.B. (1990). Structural Model of Italy scale 1:500.000, sheet 1. C.N.R., *Progetto Finalizzato Geodinamica, SELCA Firenze*.
Bolin, C., Mingguo, Z., Carswell, D. A., Wilson, R. N., Qingchen, W., Zhongyan, Z., & Windley, B. F. (1995). Petrogenesis of ultrahigh-pressure rocks and their country rocks at Shuanghe in Dabieshan, central China. *European Journal of Mineralogy, 7*(1), 119–138.
Bousquet, R., Oberhänsli, R., Goffé, B., Wiederkehr, M., Koller, F., Schmid, S. M., Schuster, R., Engi, M., Berger, A., & Martinotti, G. (2008). Metamorphism of metasediments at the scale of an orogen: A key to the Tertiary geodynamic evolution of the Alps. *Geological Society, London, Special Publications, 298*(1), 393–411.
Bucher, K., Weisenberger, T. B., Klemm, O., & Weber, S. (2019). Decoding the complex internal chemical structure of garnet porphyroblasts from the Zermatt area, Western Alps. *Journal of Metamorphic Geology, 37*(9), 1151–1169.
Burov, E., Francois, T., Yamato, P., & Wolf, S. (2014). Mechanisms of continental subduction and exhumation of HP and UHP rocks. *Gondwana Research, 25*(2), 464–493.
Caron, J. M. (1971). Contribution à l'étude lithostratigraphique et structurale de la région de Sestrière (Alpes Cottiennes, Italie). *Trav. Lab. Géol. Grenoble, 21*, 45–68.
Caron, J. M., & Saliot, P. (1969). Nouveaux gisements de lawsonite et de jadeite dans les alpes franco-italiennes. *Comptes Rendus De L'académie Des Sciences Paris, 268*, 3153–3156.
Chopin, C., Henry, C., & Michard, A. (1991). Geology and petrology of the coesite-bearing terrain, Dora Maira Massif, Western Alps. *European Journal of Mineralogy, 3*, 263–291.
Compagnoni, R. (1977). The Sesia-Lanzo Zone: High pressure-low temperature metamorphism in the Austroalpine continental margin. *Rendiconti Società Italiana Di Mineralogia e Petrologia, 33*(1), 335–374.
Compagnoni, R. (2003). HP metamorphic belt of the western Alps. *Episodes, 26*(3), 200–204.
Compagnoni, R., Rolfo, F., Groppo, C., Hirajima, T., & Turello, R. (2012). Geological map of the ultra-high pressure Brossasco-Isasca unit (Western Alps, Italy). *Journal of Maps, 8*(4), 465–472.
Connolly, J. A. D. (1990). Multivariable phase diagrams: An algorithm based on generalized thermodynamics. *American Journal of Science, 290*, 666–718.
Connolly, J. A. D. (2005). Computation of phase equilibria by linear programming: A tool for geodynamic modeling and its application to subduction zone decarbonation. *Earth and Planetary Science Letters, 236*(1–2), 524–541.
Connolly, J. A. D. (2009). The geodynamic equation of state: What and how. *Geochemistry, Geophysics, Geosystems, 10*(10), 1–19.
Corno, A., Mosca, P., Borghi, A., & Gattiglio, M. (2019). Lithostratigraphy and petrography of the Monte Banchetta-Punta Rognosa oceanic succession (Troncea and Chisonetto Valleys, Western Alps). *Ofioliti, 44*(2), 83–95.
Corno, A., Mosca, P., Gattiglio, M., & Borghi, A. (2021). Geological map of the Monte Banchetta – Punta Rognosa area (Troncea valley, Western Alps). *Journal of Maps, 17*(2), 150–160.
Coward, M.P. & Dietrich, D. (1989). Alpine tectonics: an overview. In: Coward, M.P., Dietrich, D. & Park, R.G. (eds.), Alpine tectonics. *Geological Society, London, Special Publications*, 45, 1–29.
Cuthbert, S. J., Carswell, D. A., Krogh-Ravna, E. J., & Wain, A. (2000). Eclogites and eclogites in the Western Gneiss region Norwegian Caledonides. *Lithos, 52*(1–4), 165–195.
Dal Piaz, G.V. (2010). The Italian Alps: a journey across two centuries of Alpine geology . In: Beltrando, M., Peccerillo, A., Mattei, M., Conticelli, S. and Doglioni, C. (Eds.), The Geology of Italy: tectonics and life along plate margins, *Journal of the Virtual Explorer, Electronic Edition*, 36, paper 8.
Dal Piaz, G. V., Hunziker, J. C., & Martinotti, G. (1972). La Zona Sesia-Lanzo e l'evoluzione tettonico-metamorfica delle Alpi nordoccidentali interne. *Memorie Della Società Geologica Italiana, 11*(4), 433–462.
Evans, B. W. (1990). Phase relations of epidote-blueschists. *Lithos, 25*, 3–23.
Fuhrman, M. L., & Lindsley, D. H. (1988). Ternary-Feldspar Modeling and Thermometry. *American Mineralogist, 73*(3–4), 201–215.
Ganne, J., Bertrand, J. M., & Fudral, S. (2005). Fold interference pattern at the top of basement domes and apparent vertical extrusion of HP rocks (Ambin and South Vanoise massifs, Western Alps). *Journal of Structural Geology, 27*(3), 553–570.
Gasco, I., Borghi, A., & Gattiglio, M. (2011). P-T Alpine metamorphic evolution of the Monte Rosa nappe along the Piedmont Zone boundary (Gressoney Valley, NW Italy). *Lithos, 127*, 336–353.
Ghignone, S., Borghi, A., Balestro, G., Castelli, D., Gattiglio, M., & Groppo, C. (2020). HP tectono-metamorphic evolution of the Internal Piedmont Zone in Susa Valley (Western Alps): New petrologic insight from garnet+ chloritoid-bearing micaschists and Fe–Ti metagabbro. *Journal of Metamorphic Geology*. https://doi.org/10.1111/JMG.12574
Giacometti, F., & Rebay, G. (2013). Structural and petrological evolution of the Beth-Ghinivert zone (Schistes Lustres—Italian Western Alps). *Rendiconti Online Della Società Geologica Italiana, 29*, 70–73.
Goldstein, J. I., Newbury, D. E., Michael, J. R., Ritchie, N. W., Scott, J. H. J., & Joy, D. C. (2017). *Scanning electron microscopy and X-ray microanalysis*. Springer.
Green, E., Holland, T., & Powell, R. (2007). An order-disorder model for omphacitic pyroxenes in the system jadeite-diopside-hedenbergite-acmite, with applications to eclogitic rocks. *American Mineralogist, 92*(7), 1181–1189.
Green, E. C. R., White, R. W., Diener, J. F. A., Powell, R., Holland, T. J. B., & Palin, R. M. (2016). Activity–composition relations for the calculation of partial melting equilibria in metabasic rocks. *Journal of Metamorphic Geology, 34*(9), 845–869.
Groppo, C., Beltrando, M., & Compagnoni, R. (2009). P-T path of the UHP Lago di Cignana and adjoining HP meta-ophiolitic units: Insights into the evolution of subducting tethyan slab. *Journal of Metamorphic Geology, 27*, 207–231.
Groppo, C., Ferrando, S., Gilio, M., Botta, S., Nosenzo, F., Balestro, G., Festa, A., & Rolfo, F. (2019). What's in the sandwich? New P-T constraints for the (U) HP nappe stack of southern Dora-Maira Massif (Western Alps). *European Journal of Mineralogy, 31*(4), 665–683.
Groppo, C., Lombardo, B., Rolfo, F., & Pertusati, P. (2007). Clockwise exhumation path of granulitized eclogites from the Ama Drime range (Eastern Himalayas). *Journal of Metamorphic Geology, 25*(1), 51–75.
Groppo, C., Rolfo, F., Sachan, H. K., & Rai, S. K. (2016). Petrology of blueschist from the Western Himalaya (Ladakh, NW India): Exploring the complex behavior of a lawsonite-bearing system in a paleo-accretionary setting. *Lithos, 252*, 41–56.
Guillot, S., Hattori, K., Agard, P., Schwartz, S., & Vidal, O. (2009). Exhumation processes in oceanic and continental subduction contexts: a review. *Subduction zone geodynamics*, 175–205.
Guiraud, M., Holland, T. J. B., & Powell, R. (1990). Calculated mineral equilibria in the greenschist-blueschist-eclogite facies in Na2OFeO-MgO-Al2O3-SiO2-H2O: Methods, results and geological applications. *Contribution to Mineralogy and Petrology, 104*, 85–98.
Hacker, B. R., Andersen, T. B., Johnston, S., Kylander-Clark, A. R., Peterman, E. M., Walsh, E. O., & Young, D. (2010). High-temperature deformation during continental-margin subduction & exhumation: The ultrahigh-pressure Western Gneiss Region of Norway. *Tectonophysics, 480*(1–4), 149–171.
Hawthorne, F. C., Oberti, R., Harlow, G. E., Maresch, W. V., Martin, R. F., Schumacher, J. C., & Welch, M. D. (2012). Nomenclature of the amphibole supergroup. *American Mineralogist, 97*(11–12), 2031–2048.
Holland, T. J. B. (1980). The reaction albite = jadeite + quartz determined experimentally in the range 600–1200°C. *American Mineralogist, 65*, 129–134.
Holland, T. J. B., & Powell, R. (1998). An internally consistent thermodynamic dataset for phases of petrological interest. *Journal of Metamorphic Geology, 16*, 309–343.
Holland, T. J. B., & Powell, R. (2011). An improved and extended internally consistent thermodynamic dataset for phases of petrological interest, involving a new equation of state for solids. *Journal of Metamorphic Geology, 29*, 333–383.
Labrousse, L., Jolivet, L., Andersen, T. B., Agard, P., Hébert, R., Maluski, H., & Scharer, U. (2004). Pressure-temperature-time deformation history of the exhumation of ultra-high pressure rocks in the Western Gneiss Region, Norway. *Special Papers-Geological Society of America*, 155–184.
Lanari, P., Guillot, S., Schwartz, S., Vidal, O., Tricart, P., Riel, N., & Beyssac, O. (2012). Diachronous evolution of the alpine continental subduction wedge: Evidence from P-T estimates in the Briançonnais Zone houillère (France–Western Alps). *Journal of Geodynamics, 56*, 39–54.

Lanari, P., Riel, N., Guillot, S., Vidal, O., Schwartz, S., Pêcher, A., & Hattori, K. H. (2013). Deciphering high-pressure metamorphism in collisional context using microprobe mapping methods: Application to the Stak eclogitic massif (northwest Himalaya). *Geology, 41*(2), 111–114.
Laskowski, A. K., Kapp, P., Vervoort, J. D., & Ding, L. (2016). High-pressure Tethyan Himalaya rocks along the India-Asia suture zone in southern Tibet. *Lithosphere, 8*(5), 574–582.
Leake, B. E. (1978). Nomenclature of amphiboles. *American Mineralogist, 63*(11–12), 1023–1052.
Lemoine, M., De Graciansky, P.C. & Tricart, P. (2000). De l'océan à la chaîne de montagnes. *Tectonique Des Plaques Dans les Alpes*. Gordon and Breach, Paris.
Lewis, A. D., & Snewing, J. D. (1980). The Montgenèvre ophiolite (Hautes-Alpes, France): Metamorphism and trace element geochemistry of the volcanic sequence. *Chemical Geology, 28*, 291–306.
Malusà, M. G., Mosca, P., Borghi, A., Dela Pierre, F., & Polino, R. (2002). Approccio multidisciplinare per la ricostruzione dell'assetto tettono-stratigrafico e dell'evoluzione metamorfico-strutturale di un settore di catena orogenica: l'esempio dell'Alta Valle di Susa (Alpi Occidentali). *Bollettino Della Società Geologica Italiana, 57*, 249–257.
Manatschal, G., Sauter, D., Karpoff, A. M., Masini, E., Mohn, G., & Lagabrielle, Y. (2011). The Chenaillet ophiolite in the French/Italian Alps: An ancient analogue for an oceanic core complex? *Lithos, 124*(3–4), 169–184.
Manzotti, P., Ballèvre, M., Zucali, M., Robyr, M., & Engi, M. (2014a). The tectono-metamorphic evolution of the Sesia-Dent Blanche nappes (internal Western Alps): Review and synthesis. *Swiss Journal of Geosciences, 107*(2), 309–336.
Manzotti, P., Pitra, P., Langlade, M., & Ballèvre, M. (2014b). Constraining P-T conditions during thrusting of a higher pressure unit over a lower pressure one (Gran Paradiso, Western Alps). *Journal of Metamorphic Geology, 33*, 981–1002.
Manzotti, P., Bosse, V., Pitra, P., Robyr, M., Schiavi, F., & Ballèvre, M. (2018). Exhumation rates in the Gran Paradiso Massif (Western Alps) constrained by in situ U-Th-Pb dating of accessory phases (monazite, allanite and xenotime). *Contributions to Mineralogy and Petrology, 173*(3), 1–28.
Mével, C., Caby, R., & Kienast, J.-R. (1978). Amphibolite facies conditions in the oceanic crust: Example of amphibolized flaser-gabbro and amphibolites from the Chenaillet ophiolite massif (Hautes Alpes, France). *Earth and Planetary Science Letters, 39*, 98–108.
Michard, A., Avigad, D., Goffé, B., & Chopin, C. (2003). The high-pressure metamorphic front of the south Western Alps (Ubaye-Maira transect, France, Italy). *Schweizerische Mineralogische Und Petrographische Mitteilungen, 84*, 215–235.
Michard, A., Goffe, B., Chopin, C., & Henry, C. (1996). Did the Western Alps develop through an Oman-type stage? The geotectonic setting of high-pressure metamorphism in two contrasting Tethyan transects. *Eclogae Geologicae Helveticae, 89*, 43–80.
Mohn, G., Manatschal, G., Muntener, O., Beltrando, M., & Masini, E. (2010). Unravelling the interaction between tectonic and sedimentary processes during lithospheric thinning in the Alpine Tethys Margins. *International Journal of Earth Sciences, 99*, 75–101.
Nakamura, D., & Hirajima, T. (2000). Granulite-facies overprinting of ultrahigh-pressure metamorphic rocks, northeastern Su-Lu region, eastern China. *Journal of Petrology, 41*(4), 563–582.
Nitsch, K. H. (1971). Stabilitatsbeziehungen von Prehnit- und Pumpellyit-haltiger Paragenesen. *Contributions to Mineralogy and Petrology, 30*, 240–260.
O'Brien, P. J. (2019). Eclogites and other high-pressure rocks in the Himalaya: A review. *Geological Society, London, Special Publications, 483*(1), 183–213.
Okay, A. I., Xu, S., & Sengor, A. C. (1989). Coesite from the Dabie Shan eclogites, central China. *European Journal of Mineralogy, 1*(4), 595–598.
Petrakakis, K., & Dietrich, H. (1985). MINSORT: A program for the processing and archivation of microprobe analysis of silicate and oxide minerals. *Neues Jahrbuch Für Mineralogie Abhandlungen, 8*, 379–384.
Pognante, U., & Kienast, J. R. (1987). Blueschist and Eclogite Transformations in Fe-Ti Gabbros: A Case from the Western Alps Ophiolites. *Journal of Petrology, 28*, 271–329.
Poli, S., & Schmidt, M. W. (1995). H2O transport and realase in subsuction zones: Experiemental constraints on basaltic and andesitic systems. *Journal of Geophysical Research, 100*, 22299–22314.
Polino, R., Borghi, A., Carraro, F., Dela Pierre, F., Fioraso, G., and Giardino, M. (2002). Note illustrative della Carta Geologica d'Italia alla scala 1: 50.000, F. 132–152–153 "Bardonecchia". *Regione Piemonte, Direzione Regionale dei servizi Tecnici di Prevenzione. Litografia Geda*, Nichelino. Torino.
Polino, R., Dal Piaz, G. V., & Gosso, G. (1990). – Tectonic erosion at the Adria margin and accretionary process for the Cretaceous orogeny of the Alps. *Mémoires De La Société Géologique De France, 165*, 345–367.
Powell, R., & Holland, T. J. B. (1990). An enlarged and updated internally consistent thermodynamic data-set with uncertainties and correlations: The system K2O-Na2O-CaO-MgOMnO-FeO-Fe2O3-Al2O3-TiO2-C-H-O2. *Journal of Metamorphic Geology, 8*, 89–124.
Rao, B. B., & Johannes, W. (1979). – Further data on the stability of staurolite + quartz and related assemblages. *Neues Jahrbuch Für Mineralogie Abhandlungen, 10*, 437–447.
Reed, S. J. B. (2005). *Electron microprobe analysis and scanning electron microscopy in geology*. Cambridge University Press.
Regis, D., Rubatto, D., Darling, J., Cenki-Tok, B., Zucali, M., & Engi, M. (2014). Multiple metamorphic stages within an eclogite-facies terrane (Sesia Zone, Western Alps) revealed by Th-U-Pb petrochronology. *Journal of Petrology, 55*, 1429–1456.
Reinecke, T. (1998). Prograde high-to ultrahigh-pressure metamorphism and exhumation of oceanic sediments at Lago di Cignana, Zermatt-Saas Zone, western Alps. *Lithos, 42*(3–4), 147–189.
Rubatto, D., & Hermann, J. (2001). Exhumation as fast as subduction? *Geology, 29*, 3–6.
Schmid, S. M., & Kissling, E. (2000). The arc of the western Alps in the light of geophysical data on deep crustal structure. *Tectonics, 19*, 62–85.
Schwartz, S., Lardeaux, J. M., & Tricart, P. (2000). La zone d'Acceglio (Alpes Cottiennes). Un nouvel exemple de croûte continentale éclogitisée dans les Alpes occidentales. *Comptes Rendus De L'académie Des Sciences, 330*, 859–866.
SERVIZIO GEOLOGICO D'ITALIA (2002) Carta Geologica d'Italia alla scala 1:50.0000, F. 154 Susa, Regione Piemonte, Direzione Regionale dei servizi Tecnici di Prevenzione. Litografia Geda, Nichelino. Torino.
SERVIZIO GEOLOGICO D'ITALIA (2020) Carta Geologica d'Italia alla scala 1:50.0000, F. 171 Cesana. http://www.isprambiente.gov.it/Media/carg/171_CESANA_TORINESE/Foglio.html
Smye, A.J., Greenwood, L.V. & Holland, T.J.B. (2010). Garnet–chloritoid–kyanite assemblages: eclogite facies indicators ofsubduction constraints in orogenic belts. *Journal of Metamorphic Geology, 28*, 753–768. https://doi.org/10.1111/j.1525-1314.2010.00889.x.
Stampfli, G.M. & Marchant, R.H. (1997). Geodynamics evolution of the Tethyan margins of the Western Alps. In: Lehner, P., Heitzman, P., Frei, W., Horstmeyer, H., Mueller, S., Pfiffner, A. & Steck, A. (Eds.), Deep Structure of Switzerland. Results from NRP 20, *Birkhaeuser-Verlag*, Basel, 223–239.
Strzerzynski, P., Guillot, S., Leloup, P. H., Arnaud, N., Vidal, O., Ledru, P., Courrioux, G., & Darmendrail, X. (2012). Tectono-metamorphic evolution of the Briançonnais zone (Modane-Aussois and southern Vanoise units, Lyon Turin transect, western alps). *Journal of Geodynamics, 56*, 55–75.
Wain, A. (1997). New evidence for coesite in eclogite and gneisses: Defining an ultrahigh-pressure province in the Western Gneiss region of Norway. *Geology, 25*(10), 927–930.
White, R. W., Powell, R. O. G. E. R., Holland, T. J. B., Johnson, T. E., & Green, E. C. R. (2014). New mineral activity–composition relations for thermodynamic calculations in metapelitic systems. *Journal of Metamorphic Geology, 32*(3), 261–286.
Whitney, D. L., & Evans, B. W. (2010). Abbreviations for names of rock-forming minerals. *American Mineralogist, 95*(1), 185–187.
Zhang, R. Y., Hirajima, T., Banno, S., Cong, B., & Liou, J. G. (1995). Petrology of ultrahigh-pressure rocks from the southern Su-Lu region, eastern China. *Journal of Metamorphic Geology, 13*(6), 659–675.

Publisher's Note